

Air Force Institute of Technology

AFIT Scholar

Theses and Dissertations

Student Graduate Works

3-2-2007

Biological Cell Identification by Integrating Micro-fluidics, Electrical Impedance Spectroscopy and Stochastic Estimation

Karl R. Schwenn

Follow this and additional works at: <https://scholar.afit.edu/etd>



Part of the [Biomedical Engineering and Bioengineering Commons](#), and the [Electrical and Electronics Commons](#)

Recommended Citation

Schwenn, Karl R., "Biological Cell Identification by Integrating Micro-fluidics, Electrical Impedance Spectroscopy and Stochastic Estimation" (2007). *Theses and Dissertations*. 3141.
<https://scholar.afit.edu/etd/3141>

This Thesis is brought to you for free and open access by the Student Graduate Works at AFIT Scholar. It has been accepted for inclusion in Theses and Dissertations by an authorized administrator of AFIT Scholar. For more information, please contact richard.mansfield@afit.edu.



BIOLOGICAL CELL IDENTIFICATION BY INTEGRATING
MICRO-FLUIDICS, ELECTRICAL IMPEDANCE SPECTROSCOPY AND
STOCHASTIC ESTIMATION

THESIS

Karl R. Schwenn, Captain, USAF

AFIT/GE/ENG/07-20

DEPARTMENT OF THE AIR FORCE
AIR UNIVERSITY

AIR FORCE INSTITUTE OF TECHNOLOGY

Wright-Patterson Air Force Base, Ohio

APPROVED FOR PUBLIC RELEASE; DISTRIBUTION UNLIMITED.

The views expressed in this thesis are those of the author and do not reflect the official policy or position of the United States Air Force, Department of Defense, or the United States Government.

AFIT/GE/ENG/07-20

BIOLOGICAL CELL IDENTIFICATION BY INTEGRATING
MICRO-FLUIDICS, ELECTRICAL IMPEDANCE SPECTROSCOPY AND
STOCHASTIC ESTIMATION

THESIS

Presented to the Faculty

Department of Electrical and Computer Engineering

Graduate School of Engineering and Management

Air Force Institute of Technology

Air University

Air Education and Training Command

In Partial Fulfillment of the Requirements for the
Degree of Master of Science in Electrical Engineering

Karl R. Schwenn, B.S. E.C.E.

Captain, USAF

March 2007

APPROVED FOR PUBLIC RELEASE; DISTRIBUTION UNLIMITED.


AFIT/GE/ENG/07-20

BIOLOGICAL CELL IDENTIFICATION BY INTEGRATING
MICRO-FLUIDICS, ELECTRICAL IMPEDANCE SPECTROSCOPY AND
STOCHASTIC ESTIMATION

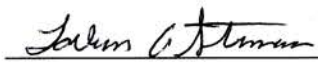
Karl R. Schwenn, B.S. E.C.E.

Captain, USAF


Approved:



Lt Col Juan R. Vasquez (Chairman) 2 Mar 07
Date



Maj LaVern A. Starman (Member) 2 Mar 07
Date



Dr. Saber M. Hussain (Member) 2 Mar 07
Date

Abstract

There is need for more precise sensing and detecting equipment for many biomedical applications. The integration of micro-fluidics, electrical impedance spectroscopy and stochastic estimation will lead to a device with enhanced detection capabilities. The goal of this thesis was to build a micro-fluidic electrical impedance measurement device that can be used in combination with a stochastic estimator to accurately identify living cells. A microdevice capable of making impedance measurements on individual living cells was designed and built using a series of standard microelectronic fabrication techniques. A microchannel was patterned in SU-8 photoresist between two gold microelectrodes on a two inch Pyrex 7740 wafer. The design process, the fabrication techniques for the microchannel, the fluid port fabrication and the cover slip bonding processes are described in detail. Small glass cover slips were bonded to the wafer using Loctite 3301 adhesive. Impedance measurements of single cells, in the microchannel device, were made using a HP4194A impedance analyzer.

Preliminary analysis of the impedance data suggests that Jurkat cells have characteristic impedance signatures, corresponding to their cell type. The microdevice that was designed and built for this project should facilitate future work to implement a stochastic estimation algorithm capable of single cell identification.

Acknowledgements

Thank you to my academic advisor Lt Col Juan Vasquez for his unwavering support and expert advice during this thesis effort. Dr. Vasquez's knowledge, understanding and optimistic outlook ensured the success of this project. I am also indebted to Maj LaVern Starman for the kind direction and guidance that he provided throughout the device design and fabrication processes. Dr. Saber Hussain and his Biological Interaction of Nanomaterials (BIN) group in the Air Force Research Lab Human Effectiveness Division deserve credit for enabling all of the biological aspects of the project.

I am especially grateful for the eager assistance given by BIN group members: Amanda Schrand, "the lab general", who helped keep the project on track and Kathy Szczublewski who introduced me to cell culturing. Thank you also to the Air Force Research Labs Sensors Directorate members: Lt Derrick Langley, Rebecca Cortez and James Gillespie who were instrumental during the fabrication phase of the project.

Additional praise goes to the fellow students who helped to troubleshoot device designs and who offered valuable suggestions: Maj Glen Kading, Capt Nathan Glauvitz, Capt Bryan Winningham, 1st Lt Mark Allard, and 1st Lt Matthew Johnson. I would also like thank Clint Richard Sikes, for leading the way.

Karl R. Schwenn

Table of Contents

	Page
Abstract	iv
Acknowledgements	v
List of Figures	ix
List of Tables	xi
I. Introduction	1-1
1.1 Thesis Statement	1-1
1.2 Background and Motivation	1-1
1.3 Project Description	1-2
1.4 Scope and Limitations	1-4
1.4.1 Research Scope	1-4
1.4.2 Limitations	1-6
1.5 Thesis Organization	1-6
II. Background	2-1
2.1 Introduction	2-1
2.2 Electrical Impedance Spectroscopy	2-1
2.2.1 Resistance	2-1
2.2.2 Impedance	2-2
2.2.3 Frequency Dependence	2-3
2.2.4 System Characterization	2-3
2.2.5 EIS Techniques	2-4
2.2.6 Bioimpedance	2-5
2.3 Estimation in Dynamic Systems	2-10
2.3.1 Linear Systems Theory Overview	2-10

	Page
2.3.2 Cell Electrical Response as a Linear System	2-11
2.3.3 Stochastic Estimation	2-13
2.3.4 System Identification	2-14
2.4 Micro-fluidics	2-14
2.4.1 Impedance Spectroscopy Microdevices	2-15
2.5 Integration Work	2-16
2.6 Summary	2-17
III. Device Design and Test Equipment Setup	3-1
3.1 Micro-fluidic Device Design	3-1
3.1.1 Device Description	3-1
3.1.2 Design Philosophy	3-1
3.1.3 Design Drivers	3-2
3.1.4 System Level Decisions	3-2
3.1.5 Overview of Device Design Work	3-3
3.1.6 Macroscopic Dimensions	3-4
3.1.7 Microscopic Dimensions	3-4
3.1.8 Photolithographic Mask Design Process	3-7
3.1.9 Mask Final Designs	3-8
3.1.10 Materials	3-13
3.1.11 Fabrication Steps	3-16
3.1.12 Cover Slips	3-18
3.1.13 Fluid Ports	3-19
3.1.14 Aspiration System	3-20
3.1.15 Design Evolution	3-20
3.2 Testing Equipment Configuration	3-23
3.2.1 Impedance Analyzer	3-23
3.2.2 Instrument Control	3-24
3.3 Summary	3-24

	Page
IV. Fabrication and Testing Results and Analysis	4-1
4.1 Introduction	4-1
4.2 Micro Device Fabrication Process	4-3
4.2.1 Step by Step Micro Device Fabrication	4-3
4.2.2 Devices Constructed	4-23
4.3 Microdevice Testing	4-24
4.3.1 Cell Lines	4-25
4.3.2 Flow Tests	4-26
4.3.3 Impedance Experiment Overview	4-27
4.4 Impedance Testing Results and Analysis	4-29
4.4.1 MC-01 Procedure	4-29
4.4.2 MC-01 Impedance Results	4-29
4.4.3 MC-05 Procedure	4-30
4.4.4 MC-05 Impedance Results	4-31
4.5 Results Summary	4-32
V. Conclusions and Recommendations	5-1
5.1 Project Conclusions	5-1
5.1.1 Research Goal	5-1
5.1.2 Achievements	5-1
5.1.3 Design and Fabrication	5-1
5.1.4 Device Testing	5-2
5.2 Recommendations for Future Work	5-3
5.2.1 Micro-fluidic Device Research	5-3
5.2.2 Stochastic Estimator Research	5-4
5.3 Summary	5-5
Bibliography	BIB-1

List of Figures

Figure		Page
1.1.	Cell Modeling	1-5
2.1.	Impedance Spectroscopy Input Signals	2-5
2.2.	Common Tissue Dispersions	2-8
2.3.	Bioelectromagnetism Applications and Principles Chart	2-9
2.4.	Coulter Counter Diagram	2-11
2.5.	Cell Impedance Measurement Overview	2-12
2.6.	Micro Impedance Device by Ayliffe et. al.	2-16
2.7.	Cell Impedance Probe by Enrique Mendechevez	2-17
3.1.	Three Device Designs Top and Side Views	3-2
3.2.	Macroscopic Dimensions for Three Designs	3-4
3.3.	Neuro 2A Cell Measurements	3-5
3.4.	Microscopic Measurements of Two and Four Electrode Devices	3-6
3.5.	Microscopic Dimensions of Six Electrode Device	3-7
3.6.	Photolithography Overview Diagram	3-8
3.7.	Final Photomask Designs	3-9
3.8.	Selectable Microchannel Positioning on Mask 2	3-13
3.9.	Mask Layout Guidelines and Mask Simulations	3-14
3.10.	Final Twelve Step Fabrication Process	3-17
3.11.	Initial Device Design Concept	3-21
3.12.	Initial Mask Layouts and Guidelines	3-21
3.13.	Cartoon of Final Device Design	3-22
3.14.	Testing Equipment Setup Diagram	3-23
4.1.	Top View of MC-05 Micro Impedance Device	4-2
4.2.	Sideview of MC-05 Micro Impedance Device	4-2

Figure		Page
4.3.	Masks Produced by Photo Sciences	4-3
4.4.	Twelve Step Fabrication Process	4-4
4.5.	Ti / Au Seed Layer Patterned with SU-8	4-7
4.6.	Anomalous Lines Produced in NR9 Photoresist	4-8
4.7.	Board for Electroplating Machine	4-10
4.8.	MC-07 Microdevice Damaged After Electroplating	4-12
4.9.	Locations of Height Measurements on Microelectrode	4-13
4.10.	Half Glass Slides Used as Test Samples	4-14
4.11.	Glass Clamps Used for Drilling Cover Slips	4-17
4.12.	Loctite UV Curable Adhesive Destroying Microchannel	4-19
4.13.	Cover Slip Bonding Test Sample	4-19
4.14.	MC-06 Device with Bubble in Adhesive	4-21
4.15.	Adhesive Withdrawing from Channel Edge	4-22
4.16.	Picture of All Test Devices Fabricated	4-24
4.17.	Picture of All Devices that were Electroplated	4-25
4.18.	Device MC-04 with Build up of Cell Particles in Channel	4-27
4.19.	Flow Test With Macrophage Cells Near Microchannel in MC-04	4-28
4.20.	Impedance Testing Equipment While Performing Tests	4-28
4.21.	Average Impedance Readings Using MC-01	4-30
4.22.	A Jurkat T Cell Between Microelectrodes on MC-05	4-31
4.23.	Average Impedance Readings Using MC-05	4-32

List of Tables

Table		Page
2.1.	Micro-fluidic Platform Functions and Fabrication Techniques	2-15
3.1.	Cell Size Data from AFRL/HE	3-6
3.2.	Design Requirements for Micro-fluidic Device	3-11
3.3.	Mechanical and Electrical Properties of Pyrex Substrate	3-14
4.1.	SU-8 Metal Liftoff Process Steps	4-6
4.2.	NR9-1000PY Metal Liftoff Process Steps	4-8
4.3.	Electrode and SU-8 Heights on Electroplated Devices	4-13

BIOLOGICAL CELL IDENTIFICATION BY INTEGRATING MICRO-FLUIDICS, ELECTRICAL IMPEDANCE SPECTROSCOPY AND STOCHASTIC ESTIMATION

I. Introduction

1.1 Thesis Statement

Build a micro-fluidic electrical impedance spectroscopy device that can be used in combination with a stochastic estimator to accurately identify living cells.

1.2 Background and Motivation

Detection and identification of different cells or tissue types has a wide range of applications in the biomedical arena. There is room for improvement in the current ability to sense and discriminate between different biological material. Areas of application for this type of biosensing technology include: detection of food borne pathogens, clinical diagnosis of disease and probing the effects of chemicals or drugs on live organisms. In each of these areas there is a need for quicker, higher precision and less invasive techniques. Impedance spectroscopy can be used to extract many different types of information without damaging the sample. Micro-fluidics can be used to improve the specificity of the measurements and stochastic estimation can be used to make higher quality analysis of the data for use in detecting, diagnosing or probing. More information on micro-fluidics, impedance spectroscopy and stochastic estimation is included in Chapter II in Sections 2.2, 2.3 and 2.4.

Micro-fluidics technology can be used to miniaturize a detection device to the point where it can interact with living material on the cellular level. In some cases, such as detection involving single cells suspended in a fluid, the miniaturization may allow for higher fidelity measurements because direct contact can be made with the cells. Impedance spectroscopy is a method used to electrically characterize a material by determining the impedance response at different frequencies.

The impedance response of any material is dependant on the electrical properties of it's component parts. Different biomaterials have different chemical and physical makeups therefore they have different impedance responses. Based on this principle, it has been shown that the electrical impedance properties of biological material can be used for unique identification of some biological materials, tissues and cells.

Measurements of a cell's impedance response across a frequency range can be used for identification based on comparison with responses taken from known sources. In some cases this assessment may be able to be performed by eye. A better approach uses mathematical relationships that link the input of the system to the system output. Linear systems theory deals with the fundamentals of dynamic systems and provides the mathematical framework to model input and output relationships based on differential equations that describe system dynamics. Linear systems theory coupled with stochastic estimation theory and multiple model adaptive estimation (MMAE) theories should provide a more robust and accurate method of comparison.

Stochastic estimation theory builds on the foundations of linear systems theory and is based on the principle truth that system models are not perfect so system models should be dealt with using probability. If models are properly defined along with their probabilistic parameters, stochastic estimation can be used to take account of all available data to produce an optimal system *state* estimate. Multiple model adaptive estimation is another extension that can be used to improve state estimates by combining more than one model in the estimator. The MMAE can determine which model best fits the measurement data input into the estimator. Once the MMAE determines the best model, it will produce optimal state estimates using that system model.

This project seeks to implement a micro-fluidic device that will allow impedance data collection of sufficient quality for use with the future work of building a stochastic estimator for cell identification.

1.3 Project Description

A microdevice was designed, fabricated and tested for this project. The work done in the project is part of a larger effort to apply modern stochastic estimation and multiple

model adaptive estimation concepts to the identification of cells. The goal of this research is to produce a capability to record impedance measurements of a single cell suspended in a saline solution. A micro-fluidic device was chosen as the appropriate method to pursue the goal of interacting directly with a single cell. Work previously done here contributed to the building blocks for a biological identification scheme based on stochastic estimation of electrical impedance data from an aggregate of living cells. This follow on project attempts to improve the specificity of the measurements over the previous work done with electrical impedance spectroscopy (EIS) of cell aggregates. This thesis seeks to integrate microelectromechanical systems (MEMS) with the aforementioned technologies in a way that will provide better impedance data for model creation.

This project is a follow-on to work completed by Enrique Mendezaceves in his master's thesis entitled "Biological System Impedance Identification Using Stochastic Estimation and Control" [29]. Lt Mendezaceves explored the use of some stochastic estimation techniques on biological impedance data recorded from cell aggregates of around 70,000 cells. In the absence of available impedance measurement equipment, he used a somewhat primitive method of impedance collection consisting of a function generator and an oscilloscope. His project achieved success in proving the concept that stochastic estimation techniques can be effectively used to identify cell types.

At the conclusion of his study, Mendezaceves offered three main recommendations for future efforts on this project. The first recommendation was to use a more accurate method of experimentation and more sensitive equipment. The second recommendation was to use microelectromechanical systems (MEMS) technology to directly contact a single cell to take impedance measurements. To do this, he envisioned building a physical probe, sized to interact directly with one cell like the one shown at the end of Chapter II in Figure 2.7. The third recommendation that he offered was implementing a more sophisticated smoother algorithm or a multiple model adaptive estimator (MMAE) to improve the identification accuracy of the system. The first two recommendations are addressed by this thesis project and the outcome of this project will enable better modeling and the development of identification algorithms based on stochastic estimation theory.

Three separate classes of micro impedance spectroscopy devices were designed. One design was chosen for fabrication and four test devices plus one fully functional impedance spectroscopy microdevice were built during the course of this project. Standard micro electronics fabrication techniques were used for most of the fabrication steps for the device. A common photoresist SU-8 was used as the channel layer. SU-8 is commonly used in the construction of other custom microelectromechanical systems. Gold electrodes were electroplated to a height even with the SU-8 channel wall. The microchannel was capped with a glass cover slip and held in place with UV curable adhesive. Inlet and outlet fluid ports were connected to the cover slips.

Figure 1.1 illustrates how the microdevice fabricated for this project will be used in conjunction with electrical impedance spectroscopy to provide data for later work in creating dynamic models of measured cell types. This project was able to make the electrical impedance measurements on the living cells to support future modelling and estimator design.

The microdevice produced in this effort was used to record impedance data from a variety of substances along with live and dead Jurkat T cells. The impedance data collected suggests that this microdevice can be used to collect data adequate to develop impedance models for living cells.

New information was learned during the design, the fabrication and during the testing. The device that was produced for this project is by no means perfect but it was successful in measuring cell impedance for preliminary modeling work.

1.4 Scope and Limitations

1.4.1 Research Scope. This project is the first micro-fluidics project completed at the Air Force Institute of Technology. The micro-fluidic electrical impedance spectroscopy device produced through this effort is very similar to devices made by others and presented in the literature. This project is not intended to be at the very cutting edge of micro-fluidics, but the device paves the way for further development of micro-fluidics here at AFIT and allows future researchers here to access single cells for more sophisticated data processing.

The following is a list of research goals accomplished through this thesis:

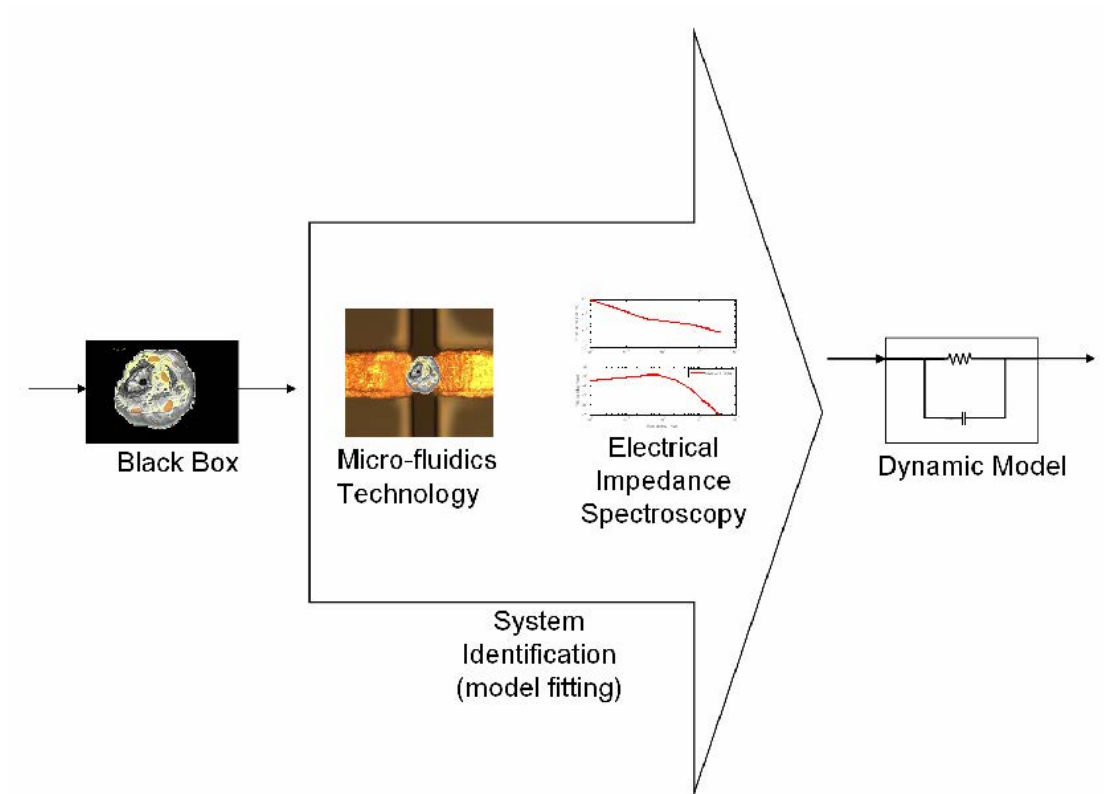


Figure 1.1 This figure displays graphically the use of the microdevice in modeling the electrical dynamics of a single cell. Through system identification techniques, dynamic models will be created to represent the electrical response measured on a certain cell type.

1. Implement an effective microchannel device design in the AFIT and AFRL cleanrooms.
2. Investigate mathematical models for electrical impedance of living cells.
3. Implement a test setup capable of taking automated impedance measurements using the microchannel device.
4. Run limited cell experiments to acquire impedance data from a living cell

The following goals were not able to be met during this thesis effort although further work in this area has been enabled:

1. Use the impedance measurement system constructed to accurately identify different cell types.
2. Compare accuracy of identification results to other systems.

1.4.2 Limitations. Some limitations existed that effected the direction that this project took. One major limitation is that the Air Force Institute of Technology has no official biological engineering curriculum. For that reason, access is restricted to necessary information and materials to conduct bioengineering projects. Bioengineering articles and print resources are hard to access on demand. Progress was slowed considerably when difficulties arose in the fabrication process. Help from researchers more familiar with micro-fluidic design and fabrication would have allowed the fabrication to progress faster.

Access to lab equipment and materials specifically for micro-fluidic design was lacking both at the AFIT and at the AFRL cleanrooms. Critical material such as photoresists along with critical equipment was borrowed from AFRL. The people at AFRL were very helpful and did their best to respond to requests as soon as their schedule allowed. However scheduling of equipment runs and obtaining photoresists were painfully time consuming. Despite these limitations, this thesis project produced a useful device for future work in this area.

1.5 Thesis Organization

This thesis is organized into five chapters: I. Introduction, II. Background, III. Device Design, IV. Device Fabrication and Test and V. Conclusions and Recommendations.

Chapter I introduces the thesis topic, describes the layout of the document and discusses the scope, major assumptions and limitations of this project. Chapter II is a summary of work done in the field and consists of a review of the current literature pertaining to the three main areas of interest for this project: EIS, MEMS and Stochastic Estimation. Chapter III describes the design of microchannel devices for this project. It also discusses the test setup used to log impedance data from single cells using the microchannel device. Chapter IV describes in detail the fabrication steps taken to construct the microchannel device and discusses the differences between design intent and the reality of construction. Also included in Chapter IV is the experimental impedance data obtained using the device and the test set up. Chapter V summarizes the results of the project and presents an assessment of the successes along with recommendations for future work at AFIT on this topic.

II. Background

2.1 Introduction

This research effort consists of an integration of technology areas. Each of the three main fields concerned: electrical impedance spectroscopy, stochastic estimation, and micro-fluidics are currently understood independently to varying degrees. This chapter provides a literature review and discussion of the background information on these disciplines.

Impedance spectroscopy has been used for many decades by researchers interested in the study of living and nonliving materials. Stochastic estimation theory in the context used here is well understood with extensive formal mathematical proofs establishing a solid foundation. The use of Stochastic estimation theory in this research is a novel application of the theory. Micro-fluidics is a subset of the emerging field of Micro Electromechanical Systems (MEMS). Of the three technology disciplines, this area is the newest and perhaps currently the least understood. Researchers in micro-fluidics are now working hard to take advantage of exciting new opportunities to interface with the environment on a microscopic scale. The following sections will describe some of the relevant work that has been done in each of the three main technology areas.

2.2 Electrical Impedance Spectroscopy

Electrical Impedance Spectroscopy (EIS) is a method of characterization for electrical networks. An impedance analyzer sweeps an input (current or voltage) signal through a range of frequencies, measures the output (voltage or current) and calculates the frequency dependant impedance. EIS can give a scientist insight into the dynamics of the system or it can simply be used to recognize one network among others because of its unique impedance response. The information that follows in this section is intended to help the reader become familiar with the principles of EIS.

2.2.1 Resistance. Resistance is a physical property of an object that quantifies the obstruction to the flow of *direct current* (DC) when an electrostatic potential is applied across the object. The concept of direct current (DC) resistance is described by Ohm's Law

$$V = IR \quad (2.1)$$

where V is the applied electrostatic potential with units of *Volts*. I is the symbol for the resulting current expressed in units of Amperes. R is the resistance of the object expressed in units of Ohms (Ω). Resistance is caused by physical interactions between flowing electrons and other particles. Examples of the interactions are collisions and the electromotive force of atomic nuclei or other charged particles. Material properties that directly effect resistance are resistivity (ρ), the cross-sectional area of the current flow path (A), and the length of the current flow path (L). Resistance is calculated using the expression

$$R = \frac{\rho L}{A} \quad (2.2)$$

The resistivity ρ is a material property that quantifies the total effect of the particle interactions causing resistance in any given material. Resistivity is expressed in units of Ohm Centimeters (Ωcm). Once the resistivity is determined for a material, the resistance of an object made from that material can be calculated using the current path dimensions and Equation 2.2.

2.2.2 Impedance. Impedance is a measure of opposition to *alternating current* (AC) flow. The term impedance is used to describe the relationship between current and voltage when the signal current is changing. Impedance, \mathbf{Z} , is expressed as

$$\mathbf{Z} = R + jX \quad (2.3)$$

where impedance, \mathbf{Z} , is a vector quantity with units of Ohms. The two dimensions of impedance are resistance, R , and reactance, X . Just as in the DC case, opposition to current flow from flowing particle interactions is described by resistance, R . In the AC case however, an additional opposition to current occurs called reactance, X . Reactance is due to momentum of the charged particles flowing as electric current and the interaction between induced electric and magnetic fields. Current direction can not change instantaneously when the applied potential changes. The ideal circuit components that show reactance are capacitors and inductors. Capacitors store charge and inductors store magnetic flux. The reactance of an ideal capacitor is $X_C = -1/\omega C$ where ω is the angular frequency of the applied signal and C is the capacitance in units of Farads (F). Inductors on the

other hand have reactance of $X_L = \omega L$ where L is the inductance in units of Henrys (H). The physical principle responsible for the inductive reactance is a negative electromotive force (emf) caused by an *induced* magnetic field. A magnetic field is always induced in the presence of a changing current. The changing magnetic field produces an emf that counteracts the applied voltage and reduces current flow thus causing impedance.

2.2.3 Frequency Dependence. As can be seen from the equations above, capacitive reactance, X_C , decreases with increasing frequency and inductive reactance, X_L , increases with frequency. In other words, a capacitor will not conduct electricity well at low frequencies but as frequency increases, the AC signal is not obstructed. Since the magnitude of the impedance is dependant on frequency, and the extent of that dependence is based on material properties (R , C and L) it follows that different materials will have unique impedance characteristics based on their material makeup. Impedance spectroscopy is simply the technique of recording impedance values across a *spectrum* of frequencies. EIS is typically used by researchers attempting to infer electrical characteristics of a system based on its characteristic impedance over the measured frequency range.

2.2.4 System Characterization. Electrical Impedance Spectroscopy or Electrochemical Impedance Spectroscopy lends itself easily to system characterization problems. It has been used most prominently as a method to characterize materials in terms of their internal electrical properties. EIS is commonly used to either test a theoretical model or to fit parameters to a model for a type of reaction that is well known [10]. For example, an area where EIS is commonly used is material corrosion studies. Standard corrosion tests such as salt spray test or quantitative analysis of dissolved metal are very time intensive. For that reason, chemists who desire to gain insight about the parameters of the chemical reactions taking place during corrosion, turn to impedance spectroscopy to determine some of the electrochemical reaction parameters.

An electrochemical process such as corrosion is usually not fully characterized by the mass transfer interaction in one electrolyte with one metal electrode. Instead, it is usually made up of many interacting "ensemble of partial elementary phenomena" [9]. In order to determine useful information, the data from coupled processes must be separated.

Claude Gabrielli gives the following examples of coupled phenomena in [10]: 1) reactive molecules in the bulk produced from chemical reactions occurring in the bulk, 2) electrodes absorbing the reactive molecules and 3) reactions at the interface. EIS is then used to separate the parameters of these fundamental processes. The separation is most easily achieved by observing the frequency response and separating the processes by their different electrochemical time constants. In an electrochemical cell (electrode / electrolyte system), when a voltage is applied, chemical reactions tend to take place on the electrodes that obey Faraday's law. There is a reduction reaction on the anode and a oxidation reaction on the cathode. There are current components due to the charge transfer associated with these reactions that can be measured. Both electrons and chemical species are transferred and contribute to the current flow in such a system. Therefore, the system becomes less straightforward than a simple electrical system.

2.2.5 EIS Techniques. The three main categories of impedance techniques are: steady state or DC, large signal analysis, and small signal analysis. The DC analysis is very limited in scope but can provide a current versus potential relationship for a given material. The large signal analysis refers to sweeping the current or voltage amplitude up and down. Small signal analysis is performed by varying the amplitude of one parameter (current or voltage) and measuring the response of the other parameter. If the system is assumed to be linear, the same results can theoretically be obtained by using a sine wave, a step function or a "white" noise perturbing signal. The criteria for system linearity and a discussion on system theory are contained in Section 2.3. Figure 2.1 displays the three different EIS techniques.

Several important parameters can be inferred from the small signal data for an electrochemical system [9]. The steady state limit of impedance at the high frequency is the electrolyte resistance. The "polarization resistance" is found by finding the limit at the low frequencies. Relaxation times of the electrochemical processes in the system are found in the mid frequencies. Relaxation times and their role in biological systems is discussed further in Section 2.2.6.3. The research in this thesis deals with the small AC signal EIS because of its advantages in the use of linear systems theory. For that reason, the other EIS techniques will not be discussed further.

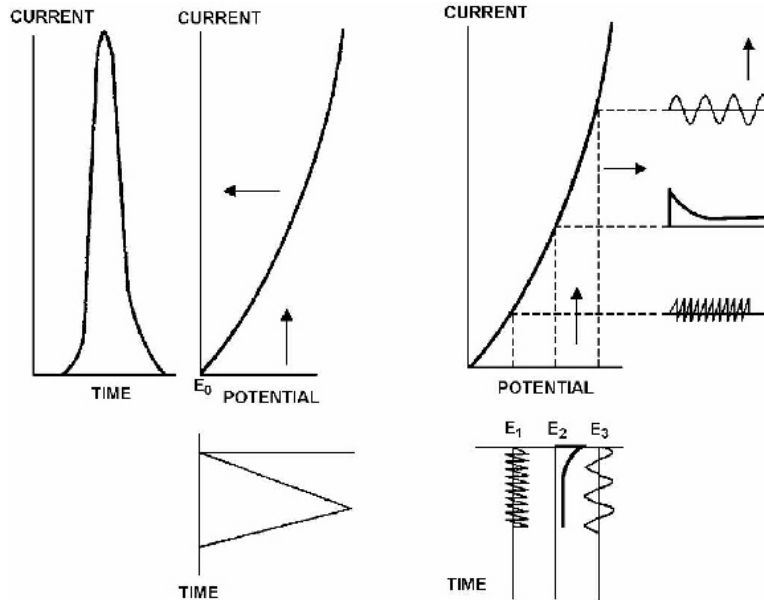


Figure 2.1 Figure from Gabrielli's Tech Note Number 24 written for Solartron Analytical [9]. Top left figure shows the resulting current for a large signal voltage sweep. The figure on the right illustrates three different perturbation signals that can be used in the small signal EIS technique: sine wave, step response and "white" noise.

Small signal EIS will be used to determine the characteristic impedance of a single cell. The use of linear system theory to create a cell model based on small signal EIS data is discussed in Section 2.3.2.

2.2.6 Bioimpedance.

2.2.6.1 History. Interestingly, the history of electricity and magnetism theory in the modern era is also the history of bioelectricity [15, 27]. Many of the founding researchers of electrical theory endeavored to understand the electrical nature of biological tissue. The first electrical devices constructed in the early 1700's were static electricity based. Two famous bioelectrical experiments carried out by Luigi Galvani were the first ever experiments dealing with flowing electricity. Galvani's first experiment resulted in the observation of the reaction of dissected frog muscle (twitching) when the nerve was touched with a metal scalpel at the same time that a static electric device was operated in the vicinity. His second experiment showed that the nerve and frog muscle could be excited merely by touching the nerve with a bronze hook grounded to an iron spike. The first experiment

revealed the electrical connection between the nerve and muscles. The second one was later explained by Alessandro Volta who invented the Volta battery based on the principle that caused DC current to flow through the frog nerve.

The years that followed brought advances in technologies and theory. The induction coil was introduced by Michael Faraday. Nikola Tesla worked with coils and capacitors to produce electric pulses which led to detection technologies able to monitor rapidly changing and small amplitude bioelectric signals such as the EEG and ECG. Hermon von Helmholtz worked on the conduction velocity in frog nerves and he also contributed superposition and reciprocity theorems which are commonly used in system theory. James Clerk Maxwell contributed the "Maxwell Equations" in 1864 adding the mathematical theory to electro-magnetism. Once the foundations of electrical theory were in place, the focus became more on specific application of the theory by biological researchers in the 20th century. ECGs and EEGs were more refined. Researchers also began to build electrical models of tissues and cell suspensions based on the insight gained by the electrical theory and pieced together using data from more and more sophisticated probing devices.

2.2.6.2 Cell Impedance Experimentation. Cell impedance experiments led researcher Rudolf Hoerber to propose the existence of a cell membranes in 1911 [15]. This was based on his observation that the resistance of blood changed with frequency which implies that blood has capacitance. He correctly surmised that the capacitance was caused by dielectric membrane. He was even able to calculate thickness of the cell membrane based on the assumption that the dielectric constant for the membrane was similar to oil. Other work in that timeframe showed that the impedance of tissue was frequency dependant as well. In 1928, Kenneth Cole began piecing together the mathematical tools necessary to model tissue impedance. He began with a tissue model based on spheres with capacitive membranes. The probing of living tissue continued with the goal of finding the principle processes giving rise to the observed data. In other words building a cell model. The Cole impedance model proposed by Kenneth Cole in 1940 is one of the most widely used cell impedance models. The model is discussed in Section 2.3.2.1. In 1941, Kenneth Cole and his brother Robert Cole authored a paper which made another advance in the understanding of the electrical behavior of living tissue. In addition to proposing an

equation that described frequency dependent permittivity in dielectrics they also included the concept of distributed relaxation times that accounted for the relaxation response of the dielectric [15].

2.2.6.3 Dispersions. A well known process referred to as relaxation occurs in a homogeneous dielectric under the influence of a changing potential. Relaxation is a term that describes the reorientation of dipole molecules after a step change in applied potential. Large dipole molecules such as some proteins have a relatively long relaxation time as compared with very small dipole molecules such as water [15]. In an alternating current, there is a frequency dependence of the ability of dipoles to reorient based on their relaxation time.

In the late 1950's Herman Schwan described a basic set of dispersions that typically take place during tissue impedance experiments of muscle cells. The dispersions are based on the assumption that well defined processes are occurring in a cell during a frequency sweep and each process is assigned an associated relaxation time. Tissue and cell cultures are made up of cell membrane, cytoplasm and various organelles. If a constant potential is applied to opposite sides of a cell, charged particles will migrate and the cell will become polarized. When working with small signal AC impedance spectroscopy as described in Section 2.2.5. The charged particles that cause the polarization of the cell or any system for that matter take time to move and to achieve this effect. The movement time is described by relaxation time. Since all cells have common features and similar internal chemistry, there are common relaxation times for all cells. This is the basis of Schwan's observation of the three dispersion events α , β , and γ shown in Figure 2.2. Schwan's α dispersion was proposed to be related to cell membrane effects, β dispersion due to outer membrane and organelle membrane capacitance and the γ dispersion was thought to be caused by relaxation of dipolar molecules in the media.

Schwan's dispersions are a step in the right direction, but it has later been realized that there are in fact a greater number of dispersions at play in a bioimpedance measurement than the three classically defined [13]. The higher order dispersions are a result of different molecular components in cells relaxing at different frequencies. For instance, the β region can be subdivided into separate β_1 and β_2 regions corresponding to different fre-

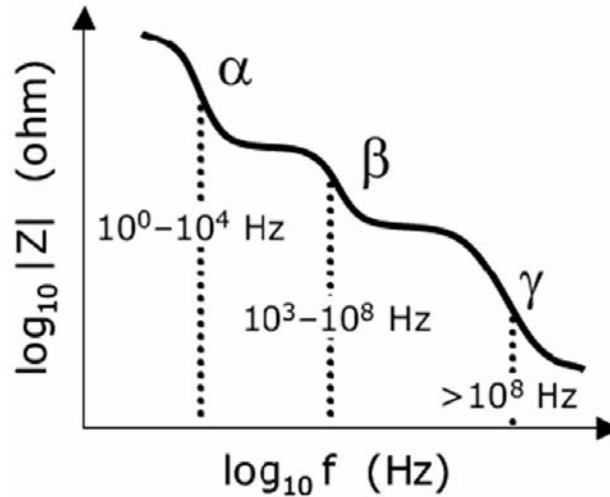


Figure 2.2 Graph showing typical alpha, beta, gamma dispersion ranges from Peter Åberg's thesis [1]. Alpha dispersion is caused by such processes as: ion interactions at the cell membrane, ions in the electrolyte diffusing and ionic connections between cells. Beta diffusion is caused by attributes such as intrinsic cell membrane capacitance and capacitances of organelles. Gamma dispersion in the very high frequency range is attributed to relaxation of water, salts and suspended proteins [15].

quencies of occurrence. There has also been a discovery of a δ dispersion in the Gigahertz range [1]. Low frequency impedance data in the α region (from 0 to $1kHz$) is difficult to interpret because dispersions in this frequency band are a result of many simultaneous physical processes. Dispersions in the α region include: electrode polarization, electroosmotic convection relaxations, particle electrophoresis and electrochemical interactions [13,37]. Due to the measurement and interpretation difficulties at the upper and lower frequency ranges, much of the current literature deals with the β range for characterizing biological material.

2.2.6.4 Other Modern Uses of Bioimpedance. Impedance plethysmography is the use of bioimpedance measurements of body structures like organs or limbs to monitor blood volume changes. This effect was first documented by Jan Nyboer in 1940 and has since been further validated and the effects characterized [22]. Impedance plethysmography systems work based on the fact that different tissues have different electrical properties and thus different impedance. Body water and tissue composition can be determined from impedance data. Figure 2.3 graphically depicts the major areas of bioelectromagnetism

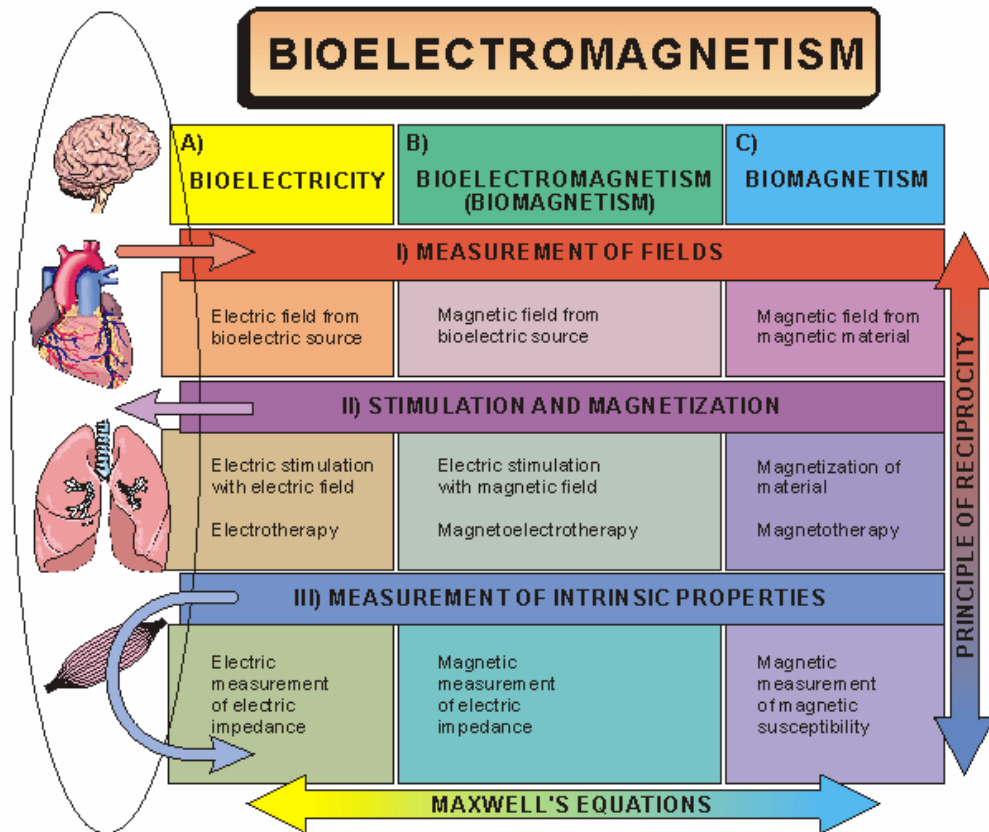


Figure 2.3 Illustrated chart from [26] shows the common applications and principles of bioelectromagnetism. This thesis is focused on the A)-III) block "Electric Measurement of Electric Impedance". The rest of the chart shows the breadth of the bioelectromagnetism field.

study today. Electric impedance measurements are only one facet of the overall field of bioelectromagnetism

Impedance plethysmography was used in a particularly interesting way in Peter Åberg's Doctoral Thesis at the Karolinska Institutet in Stockholm entitled "Skin Cancer as Seen by Electrical Impedance" [1]. The thesis describes Åberg's experiments to detect skin cancer in patients at the Huddinge University Hospital in Sweden. This example shows the breadth of possible uses for impedance probing techniques. Åberg's results were positive as he was able to detect skin cancer using his impedance techniques with a "clinically significant" accuracy.

An example of the lasting importance of cell identification and the impact of bioimpedance on the medical field is the Coulter Counter designed by Wallace Coulter in 1953.

The Coulter Counter is a simple and elegant device that uses differential impedance measurements to size and count particles suspended in a liquid. Until 1953, hospital laboratories around the world relied on manual counting and identification of blood samples for blood work like the Complete Blood Cell Count (CBC). The (CBC) is the most common blood test today because it is so useful as a first order indicator of cause of illness. A diagram of the Coulter Counter is shown in Figure 2.4. The Coulter Counter works by drawing an electrolyte containing suspended particles through a tiny aperture which separates a cathode and an anode. The two electrodes are immersed in an electrolyte solution with particles in suspension. The anode contacts the main electrolyte bath and the cathode contacts electrolyte inside an insulated tube. A particle passing through the aperture causes an increase in resistance because the cross-sectional area of the opening is decreased. The change in resistance is proportional to the volume of the cell and can be approximated by the simple expression

$$\Delta R = \frac{\rho_{electrolyte} \times V_{particle}}{A^2} \quad (2.4)$$

Where $\rho_{electrolyte}$ is the resistivity of the electrolyte, $V_{particle}$ is the volume of the particle and A is the cross-sectional area of the opening.

2.3 Estimation in Dynamic Systems

2.3.1 Linear Systems Theory Overview. Linear systems theory is a mathematical toolset with very broad applications. Most dynamic systems can be closely approximated by linear system models [34, 35]. Systems of any type (economic, mechanical, electrical, social or biological etc.) which undergo a change that behaves within physical laws can likely be described with a mathematical model based on the differential equations that describe the dynamics. The solution to the differential equations can link an input signal for the system to a resulting deterministic output. The advantage of working with a linear system is the availability of mathematical tools that have been developed over the years for analysis.

2.3.1.1 Inputs and Responses. Linear systems are input to output relations. The input or driving signal is used to calculate a system output or response using mathematical representations of the physical processes.

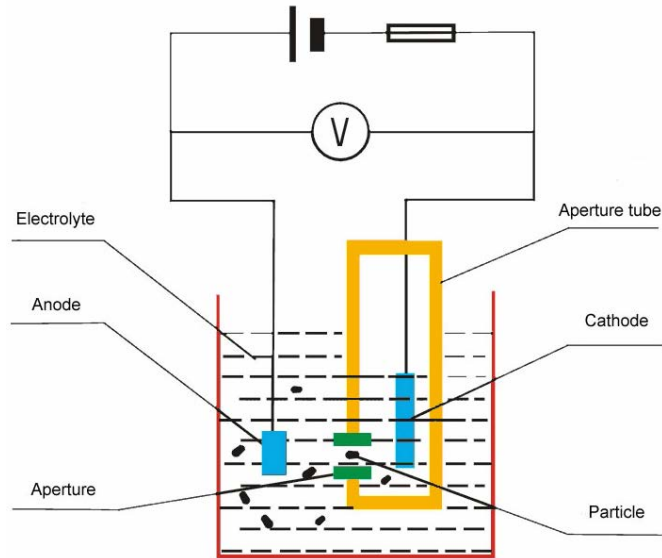


Figure 2.4 Diagram from pulvetechnology.com of a basic Coulter Counter. When voltage is applied across the electrodes, current flows from the anode to the cathode through a microscopic aperture. The particles in suspension are sensed by the current monitoring system because they increase the resistivity of the aperture as they pass through.

2.3.1.2 Conditions for Linearity. According to Katsuhiko Ogata, a system is considered linear when the principle of superposition is valid [34]. A system obeys the principle of superposition when the response to two added inputs is the same as the addition of the separate response to each input. J. Gary Ried gives more mathematically precise conditions for linear systems. He writes that there are three conditions for linearity [35]:

1. Additivity of zero-input and zero-state response
2. Linearity with respect to initial state
3. Linearity with respect to input function

The principle of superposition allows a multiple input system to be solved one input at a time thus reducing complexity.

2.3.2 Cell Electrical Response as a Linear System. An impedance spectroscopy experiment viewed as a dynamic system is basically a system governed by electrical and / or electrochemical physical laws. The input is a voltage and the output is a current. Physical laws govern the flow of current in relation to the applied voltage. Figure 2.5 illustrates the

idea of frequency dependent impedance measurements taken on a cell during an impedance spectroscopy experiment.

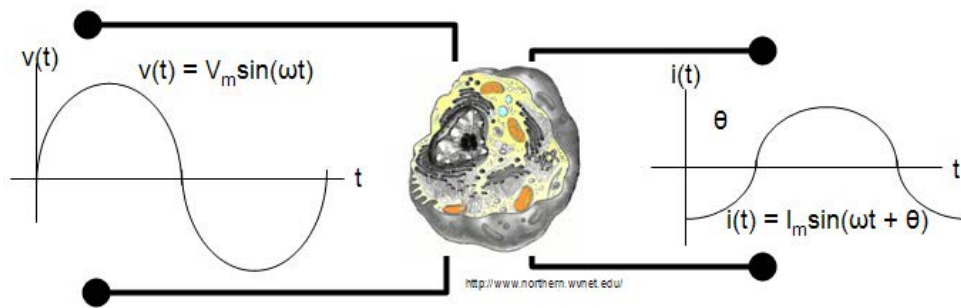


Figure 2.5 This image illustrates the process of impedance measurement of a cell. The input voltage signal is applied to the cell. The resulting current flow is measured. There is a phase change between the input voltage and the output current as well as an amplitude change. The frequency remains constant. The phase and amplitude changes represent the imaginary and real parts of the electrical impedance. This measurement is repeated over many frequencies and recorded to construct a bode plot showing the impedance change with frequency. The drawing of the cell is from <http://www.northern.wvnet.edu/>.

Different attempts have been made throughout the years to model the electrical response of living tissue. Some of the models are intended to be used to deduce what internal mechanics lead to the response. Other models are purely empirical and simply reproduce responses obtained experimentally. The correct model to use for any application must be determined taking into account the desired outcome and the necessary complexity and fidelity. For this thesis, a simplified model will be assumed. Little attention will be paid to the internal processes causing the observed response as long as characteristic models can be developed using the observed data.

Other researchers, more interested in the physical and chemical processes at work in a cell, have attempted to form models based on those internal processes to some success. The most well known and the oldest model that recreates experimental data for some cell types while also providing some insight into the mechanisms affecting tissue impedance is the Cole model.

2.3.2.1 Cole Model. The impedance of biomaterials is by nature nonlinear. The Cole model makes use of a construct called a constant phase element [19] to describe the constant phase behavior observed in bioimpedance measurements. The Cole model is

but one mathematical description of the impedance response of biomaterial. It is based on collected data and is useful to model the behavior of some cell types but does not explain the mechanisms causing the response [6, 15, 22, 26]. The Cole impedance model is given by the following equation [15, 16]:

$$\mathbf{Z} = R_{\infty} + \frac{\Delta R}{1 + (j\omega\tau_Z)^{\alpha}}, \quad \Delta R = R_0 - R_{\infty} \quad (2.5)$$

where R_0 is the DC resistance and R_{∞} is the high frequency resistance, τ_Z is the characteristic time constant corresponding to the characteristic frequency ω_Z of the system and α is an exponent. The expression $(j\omega\tau_Z)^{\alpha}$ describes a *constant phase element* when α is constant since

$$j^{\alpha} = \cos(\alpha\pi/2) - j \sin(\alpha\pi/2) \quad (2.6)$$

and $\alpha = \varphi_{CPE}/90^{\circ}$. φ_{CPE} is the constant phase angle observed from the constant phase element.

For this thesis, the cell system will be considered to be linear and time invariant. A transfer function will be created using the data collected from cell samples. The proper explanations for the modeling is beyond the scope of this thesis. For the purposes outlined in Chapter I, the cell model used is assumed to be somewhat arbitrary as long as it allows a differentiation based on different cell types. So although there are models that come close to describing the actual system behavior, this thesis will seek to create separate models based on the data collected during cell characterization experiments using the MATLAB System Identification Toolbox.

2.3.3 Stochastic Estimation. The end goal of this project is to get to the point where standard principals from the field of stochastic estimation can be used to build a cell identification estimator. System identification tools can be used to find a transfer function for the cells under test. Using models developed with that information, an estimator based on multiple model adaptive estimation can then be built. The result is a system capable of identifying different cell types based on residuals (difference between expected and actual data).

2.3.4 System Identification. In order to build a smoother or a MMAE, a dynamic model must be created. The MATLAB System Identification Toolbox (SIT) will be used in future projects to adjust parameters until a given model output compares well with the experimental data [23]. The relationship used to link the input to output in the SIT are linear difference equations. System identification can be accomplished by different methods. The process of fitting a model has three parts: input / output data collection, choice of possible models and determination of model selection criteria [23]. Detailed aspects of the SIT are not included in this thesis because it is beyond the scope.

2.4 Micro-fluidics

Micro-fluidics is a new area of micromachining technology dealing with the construction of extremely small fluid flows. The field of micro-fluidics is relatively immature when compared to microelectronics. Standard reliable architectures are still under development and as a result, considerable effort goes into designing an integrated micro-fluidic system that will perform more than one micro-fluidic function. The first micro-fluidic fabrication processes were based on techniques and equipment originally used to make microelectronics and then later adapted to microelectromechanical machines. The current trend is to build on this migration of the tools to form more reliable components and to shorten the fabrication timeliness. Table 2.1 is a list of common micro-fluidic functions that need to be implemented and validated to enable monolithic micro-fluidic designs as in the microelectronics field. The functions on the right and fabrication techniques on the left are features that a reliable micro-fluidic platform must possess. The information displayed in the table was adapted from the book *BioMEMS* Edited by Gerald Urban [12].

Micro-fluidics is a new technology area with many applications in the life sciences. It is currently possible to fabricate micro-fluidic devices able to perform many of the different functions listed in Table 2.1. Work needs to be done on integration, validation and standardization of approaches in such a way that the excessive time and cost of fabrication is reduced. Several different micro-fluidic platform concepts have been proposed such as PDMS based micro-fluidics, lab on a disk, droplet based micro-fluidics etc. [12]. Although platforms like these are without a doubt the best choice for the future of micro-fluidics, fabrication is still possible using traditional microelectronics fabrication equipment. For

Table 2.1 Micro-fluidic Platform Functions and Fabrication Techniques

Functions	Fabrication Techniques
Fluid Transport	Manufacturing technology for prototypes and mass fabrication
Fluid Metering	
Fluid Valving	Integration of components that perform functions
Fluid Mixing	
Separation	Standard easy to use packaging interconnects
Concentration	Monolithic integration capability
Detection	

labs not equipped to process using one of the new micro-fluidics platforms, the traditional fabrication methods will continue to be the only choice.

This section provides an overview of micro-fluidic devices reported in the literature and will review the fabrication process used. The intent of this literature review was to assess the techniques and materials currently being used, identify process steps possible to complete in the AFIT and AFRL cleanrooms and to gain insight into testing methodologies used on other micro EIS devices.

2.4.1 Impedance Spectroscopy Microdevices. A variety of researchers have contributed to the current state of the art micro fluidic based impedance sensing chip.

One of the earliest and most important research papers detailing fabrication of a microchannel device capable of impedance spectroscopy is "Electric Impedance Spectroscopy Using Microchannels with Integrated Metal Electrodes" written by Edward Ayliffe, A. Bruno Frazier and R. D. Rabbit all from the University of Utah [2]. The paper, published in March, 1999, outlines steps taken by the research group to build a working device using standard MEMS technology. Figure 2.6 shows the device that Ayliffe et. al. constructed. The goal was to build a system able to work directly with single living cells in solution. This research is the first step toward miniaturizing biological impedance spectroscopy in the hopes of gaining higher precision measurements of cells allowing for direct interaction with cells and opening the door to allow for collection of data representing processes going on inside of cells.

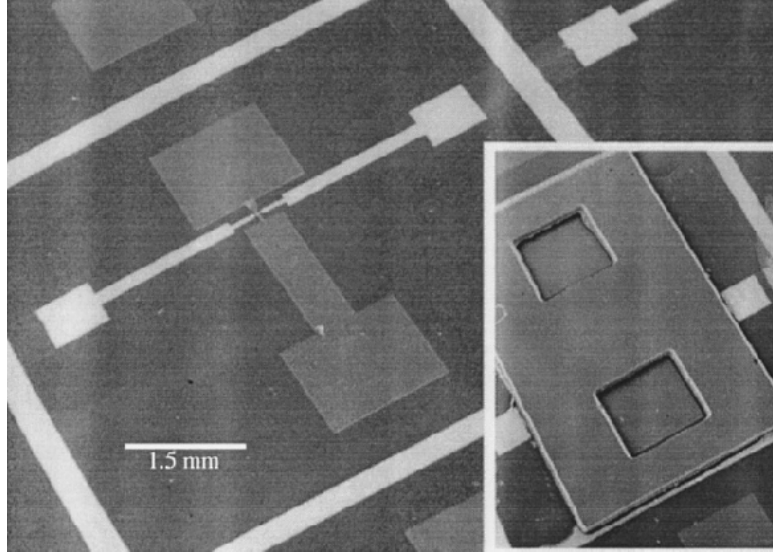


Figure 2.6 Electron Micrograph of the microdevice fabricated by Alyliffe et. al. [2]. The microchannel is shown between the two gold electrodes in the main picture. The overlay on the bottom right shows the full device with the cover slip in place.

The device that Alyliffe et. al. is effectively a short channel with a width of around $10\ \mu\text{m}$ and a height of about $4\ \mu\text{m}$. Two opposing metal electrodes protrude into the channel to provide measurement of a passing or stationary cell in the microchannel.

2.5 Integration Work

This section describes the result of a literature review on integration work (between stochastic estimation, micro-fluidics and EIS) that has already been performed. Only one known source worked directly with stochastic estimation and impedance spectroscopy and that is the work done at AFIT by Enrique Mendezaceves [29]. The integration of micro-fluidics and EIS of biological systems has been discussed by several authors [2–4, 11, 14, 18, 24, 28, 33, 36]. Figure 2.7 shows a mechanical probe envisioned by Mendezaceves. This is one possible integration with MEMS technology. A micro-fluidic device has several advantages over this mechanical device. For instance keeping the cell alive while probing with this device would be difficult. In addition, positioning the cell near the probe would require extreme effort.

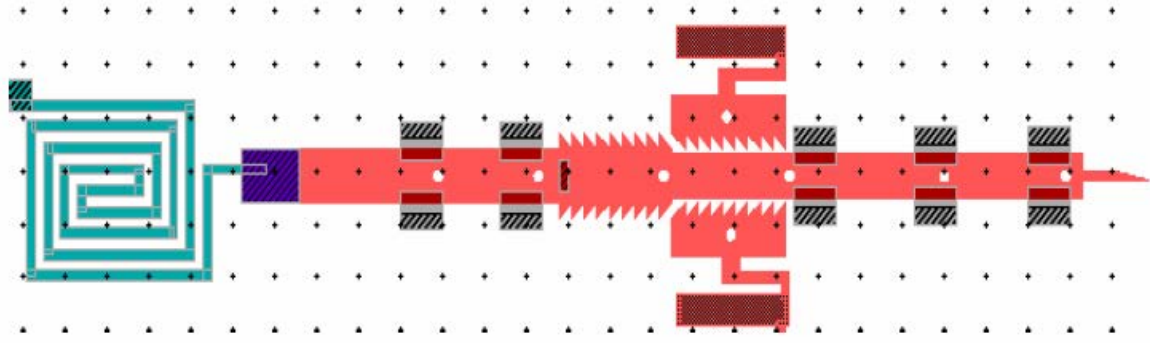


Figure 2.7 This figure shows a microprobe designed by Enrique Mendechevez but never fabricated or tested. The probe is 100 microns long and the tip has a width of 10 microns. This type of probe is somewhat impractical due to the difficulty of placing a single cell sample in range of the probe.

2.6 Summary

The three main technology areas involved in this thesis were reviewed in this chapter. Background information for stochastic estimation, electrical impedance spectroscopy and micro-fluidics were provided. The next chapter will develop the particular designs for a micro-fluidic chip as well as planning work done for the test equipment setup.

III. Device Design and Test Equipment Setup

Three micro-fluidic single cell impedance measurement devices were designed. This chapter discusses the design work performed on the microdevice. It also covers the thought process and preparation work put into the impedance sensing and recording test station setup.

3.1 Micro-fluidic Device Design

The overall goal for the microsystem design project was to build a capability for taking Electrical Impedance Spectroscopy (EIS) measurements on single cells.

3.1.1 Device Description. Three separate designs were completed. The final design drawings for all three devices are shown in Figure 3.1. The simplest design consists of two opposing electrodes that protrude into a microchannel which runs between them (see Figure 3.1 a.). This simple structure has been repeated in the literature using SU-8 based microchannels as well as channels made using other materials. In addition to the double electrode design, two other unique designs were created based on the SU-8 technology. Those two designs were never implemented due to time constraints and equipment limitations.

The two electrode design is intended to allow measurement of one live stationary cell at a time using a two point impedance analysis system. The four electrode device (see Figure 3.1 b.) is somewhat more sophisticated and allows connection directly to a four point impedance measurement system. Four point impedance measurements may be more accurate than a two point system because of the ability to remove more error from stray reactance [9]. The four electrode design also features a choice of microchannel widths for added versatility. The six electrode device (see Figure 3.1 c.) has three separate measurement sites. It was intended for possible use in positioning and detecting biological cells that are flowing in the channel. With this electrode configuration, cells could be positioned using electrophoresis using an upstream electrode pair and sensed using the downstream electrode pairs.

3.1.2 Design Philosophy. Simplicity is the key to this design. Design features such as straight channels, standard fluid interconnects, standard design dimensions between

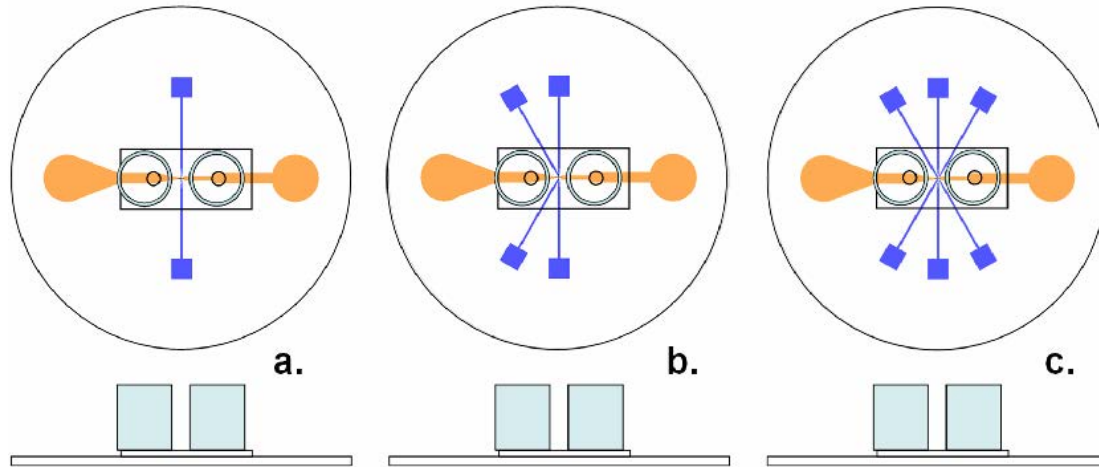


Figure 3.1 This figure shows the top view and a side view for all three final designs: a. Two electrode device, b. Four electrode device and c. Six electrode device. Each device fits on a 2 inch diameter Pyrex wafer. The wafer is shown as the circular outline around the device patterns. The recessed channel is shown in orange and runs left to right. The electrodes are shown in blue. A small cover slip is adhered in place over the channel. Two fluid port interconnects are shown adhered to each cover slip.

the devices, and one structural channel layer were all brought together to make a robust useful microdevice. The design was kept as simple as possible to increase the chances of fabrication success. Deliberate and methodical effort was put into decreasing the risk of failure during the fabrication process. The usability of the device was also of paramount concern.

3.1.3 Design Drivers. The following challenges became design drivers for the initial design:

1. Available clean rooms are configured for microelectronic fabrication and not microfluidic fabrication
2. Short time-line for design, fabrication and test
3. All major equipment necessary for the project was yet to be purchased, borrowed or scheduled

3.1.4 System Level Decisions. The following major decisions were made in the beginning of the project

1. Base design on technology used to fabricate similar micro-fluidic chips reported in the literature to reduce design risk and risk of redoing the device fabrication step.
2. Use a fabrication process with steps that are common to microelectronics fabrication. The only labs available for this project work mostly with semiconductor devices.
3. The device was designed to work on an inverted light microscope.

3.1.5 Overview of Device Design Work . The design work matured through three phases: requirement definition, initial design and requirement changes / final design. In some cases, these design phases overlapped. The device sometimes reached a certain fabrication step with a fully mature and final design for some features while the design of other features were still being modified. Some requirements were changed later in the process than would be ideal. Changes later in the project were usually based on information learned during construction and were difficult to anticipate without any previous experience in micro-fluidic work.

A systems perspective design was used as much as possible. As is common, there were a hierarchy of requirements to be implemented that ranged from very general to the most specific. System level requirements included the capability to interface with a microscopic cell, the ability to interface with macroscopic fluid lines and a design decision to use traditional microelectronic fabrication methods for the device fabrication as opposed to attempting to use other micro-fluidic specific fabrication methods. Traditional micro-electronic fabrication processes string together a customized sequence of steps to process a wafer. The steps include: photolithography to make patterns, deposition of metal layers or other materials, etching for removal of substrate material, metals and any other added layers using various acids or solvents.

The device design consisted of a photolithographic mask design including a design of all of the photolithographic steps and decisions on materials and methods to be used during those steps. The other major design areas were overall dimensions of the device, designing accessible fluid and electrical interconnects and performing assessments of utility in the biological laboratory. The following sections describe the design process in detail.

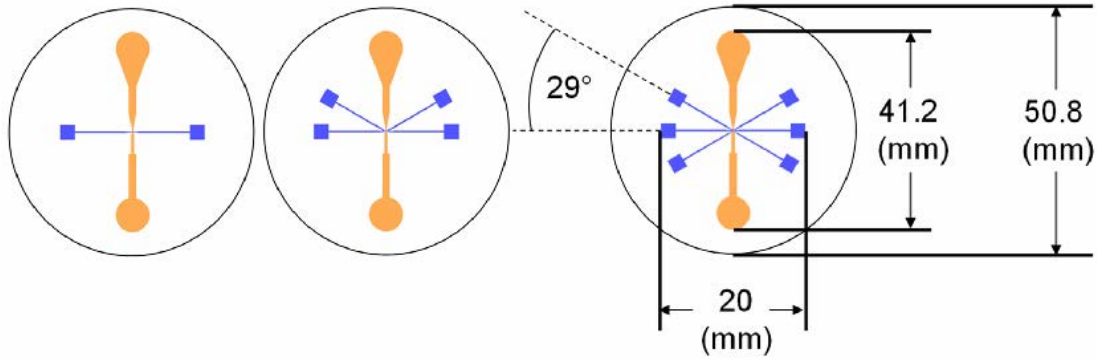


Figure 3.2 The three different device designs all share standard sizing where applicable. The overall dimensions of all three devices are 41.2 millimeters by 20 millimeters. The angled electrodes on both the four electrode and six electrode designs are at 29 degrees. The Pyrex wafers have 50.8 millimeter (2 inch) diameters.

There are several designs for impedance measurement microdevices that have been reported in the literature. Members of one class of devices reported all use SU-8 photoresist as the structural layer for the channel and they generally employ gold electrodes [2, 32]. The properties of SU-8 are described in more detail in Section 3.1.10.2. This method of device fabrication was chosen over others like Polydimethylsioxane (PDMS) because SU-8 is available in our lab. Devices of this nature can be fabricated in a standard cleanroom using microelectronic fabrication processes.

3.1.6 Macroscopic Dimensions. The overall dimensions of the device were sized to allow easy connections to macroscopic electrodes and fluid interfaces. All three designs share some standard dimensions including overall length and width, fluid port diameters, and electrode sizes. The macroscopic dimensions are shown in Figure 3.2.

3.1.7 Microscopic Dimensions. The purpose of the micro impedance device is to make measurements on a single cell. Therefore the microscopic dimensions are driven by the dimensions of the live cells that the device will be used with.

Cell sizing data was collected for two cell types which were identified by Air Force Research Laboratory Human Effectiveness Division (AFRL/HE) personnel as cell lines available for use with this project. Neuro 2A (N2A) cells and Macrophage cells were cultured in flasks and cared for according to ATCC guidelines. The neuro cells are an adherent cell line, which attach to the plastic flasks that they grow in. Trypsin (a digestive enzyme) was

used to remove the protein bonds between the cells and the flask. After adding trypsin and agitating, the cells were viewed under a light microscope. Figure 3.3 shows a picture of the neuro cells with measure bars added.

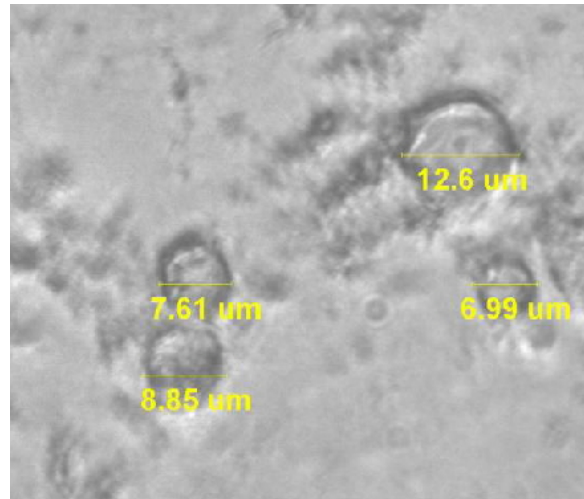


Figure 3.3 This micrograph of Neuro 2A cells was taken using a calibrated light microscope. Trypsin was added to the cell suspension to eliminate adhesion. Measure bars were added to determine the sizes of the Neuro 2A cells.

Additional sizing data was provided by a member of AFRL/HE for Macrophage cells and Neuro 2A cells. Table 3.1 shows that the cells measure between 4.2 to 19.5 microns in horizontal diameter. Cell sizing data of N2A cells obtained from the two separate sources do not completely agree. The average size and the largest cell size shown in Figure 3.3 are both larger than the average and largest sizes reported in Table 3.1. The table lists cell sizing data provided by AFRL/HE for two cell types (Macrophage and N2A). This difference between the sizing data provided and the measured size of N2A cells may be due to the calibration error on the microscope used to take measurements.

Cells in suspension are assumed to be spherical in shape based on the second law of thermodynamics. Cells that are resting on a surface may be oblong and may have a larger horizontal diameter than a vertical diameter. No data was available to estimate the heights of cells relative to their horizontal diameter. However, the assumption was made that the heights of cells were less than their horizontal diameters for the design. Neither N2A or Macrophage cells were used for the actual cell experiments. Those experiments are described in Chapter IV Section 4.3.

Table 3.1 Cell Size Data from AFRL/HE

Cell Type	No. of measured cells	Smallest	Largest	Average Size
Macrophage	41	6.2 μm	19.5 μm	10.3 μm
N2A	46	4.2 μm	7.5 μm	5.3 μm

Based on the available data for N2A and Macrophage cell sizes and based on the assumption that those two cell lines would be used for impedance interrogation, a nominal channel width of 12 μm was chosen. The two electrode microdevice was designed to have only one choice for channel width as shown in Figure 3.4. The channel widths for both the six and four electrode devices are selectable (see Figure 3.8). A channel of 10 μm , 12 μm or 15 μm can be used with these two designs. The 12 μm channel with the six electrode design is shown in Figure 3.5. The microchannel should allow only one cell at a time to enter for proper impedance measurements.

The electrode gaps on all devices (two, four and six electrode) were set to 9 μm and are not selectable for added simplicity. It was assumed that larger cells flowing through the larger microchannel would have the ability to squeeze between the 9 μm electrode gap. The electrode gap is intended to be smaller than the channel size and slightly smaller than the cell size to ensure contact by both electrodes with the cell.

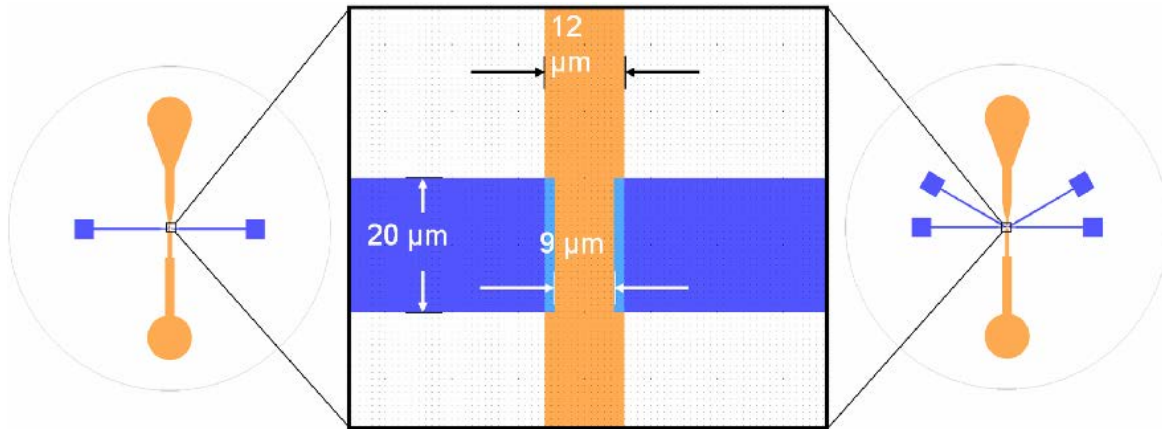


Figure 3.4 The channel and electrode dimensions are shown for the two and four electrode device designs. Both designs have the same electrode width and the same electrode gap. The two electrode design has a fixed channel width of 12 microns. The channel width on the four electrode design is selectable between 10, 12 or 15 microns.

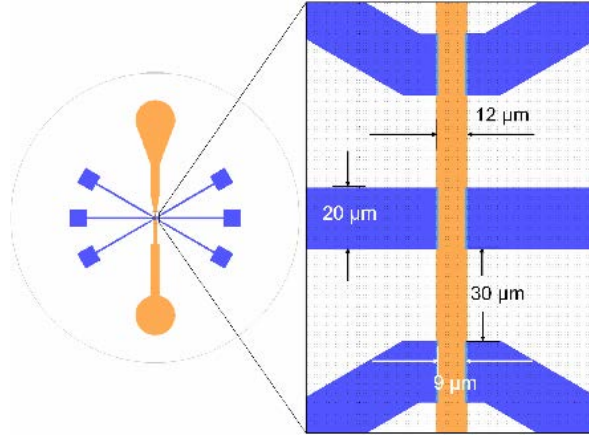


Figure 3.5 This figure shows a blowup view of the microelectrode configuration on the six electrode device. All of the electrodes are 20 microns wide and are separated in the microchannel by a 9 micron gap. Just as with the four electrode design, the channel width is selectable. The channel width shown is 12 microns.

3.1.8 Photolithographic Mask Design Process. The fabrication of the micro-fluidic device required the design and fabrication of photolithographic masks to transfer patterns onto photoresists which were used for various purposes during the fabrication process.

Photolithographic masks are central to modern semiconductor engineering. The masking process and the use of light sensitive chemical barriers called photoresists are the technology enabler that allowed electronic components to be miniaturized during the latter part of the 20th century. As the field of microelectromechanical machines grew out of the microelectronics field, manufacturing of micromachines also use the same tools. Photo masks enable a designer to selectively expose a photoresist coated substrate with UV light. With positive polarity photoresists, the resist exposed to the UV light becomes weaker due to breaking bonds. In a negative resist, more bonds are formed when it is exposed to UV light. The mask forms a pattern by selectively blocking ultraviolet light during an exposure step. After exposure, the photoresist is developed with a chemical developing solution that removes only the photoresist with weaker bonds (see Figure 3.6). Therefore, after the development step, a pattern of photoresist that matches the mask pattern is left on the substrate [20, 21, 38].

In a photolithographic fabrication process, the masks are central to the device construction. The patterns on the mask form the building blocks of features on the device. The following section describes the steps that were taken to design a set of photomasks for

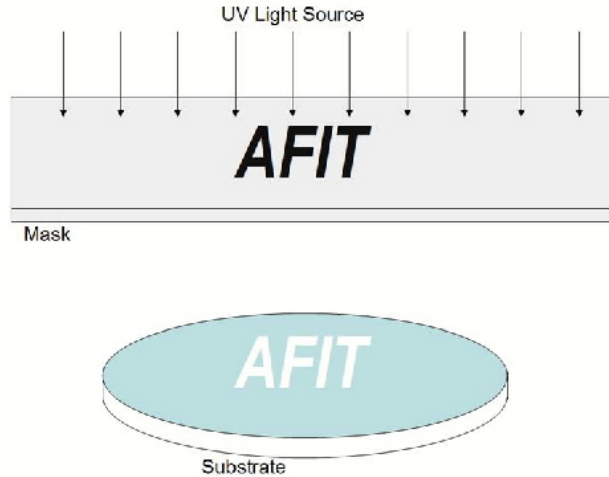


Figure 3.6 This graphic illustrates the use of a photolithographic mask with a negative photoresist for transferring a pattern. The word AFIT is patterned into the photoresist layer on the top of a substrate by selectively exposing it to ultraviolet (UV) light. The resist that was shielded from UV light by the mask pattern is removed using a chemical developer solution (white AFIT pattern on substrate). The photoresist which was exposed to the UV formed tough crosslinks and remains on the substrate despite the developer.

this thesis. Several masking steps were designed for the three microchannel devices. In an attempt to lower development cost, a total of nine separate steps were included on two masks.

3.1.9 Mask Final Designs. The layouts of the final mask designs are shown in Figure 3.7. The areas colored in orange represent the metal pattern on the mask. The masks are designed to work with negative polarity photoresists so that the areas blocked by the mask's metal layer will be removed. The necessity for the different patterns along with a description of the fabrication process flow is included in Section 3.1.11. Earlier design iterations are discussed later in Section 3.1.15.

Mask 1 contains four masking steps (listed clockwise from top middle step on Mask 1 in Figure 3.7):

1. Two electrode pattern
2. Two electrode device pattern (*with standard 12 μm wide microchannel*)
3. Four electrode pattern

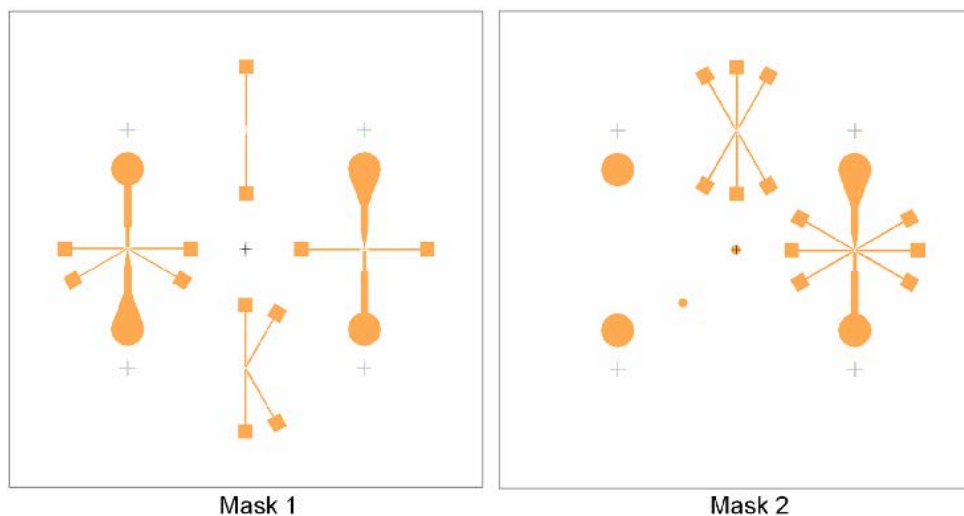


Figure 3.7 This figure shows the final mask layouts that were sent to the mask manufacturer Photo Sciences Corporation. Mask 1 on the left contains the patterns for the electrodes and channels for the two and four electrode design. Mask 2 contains the patterns for the channel and electrodes of the six electrode device along with the patterns for the port holes and selectable channels which are used only for the four and six electrode designs.

4. Four electrode device pattern (*without microchannel*)

Mask 2 also contains five separate masking steps (listed clockwise from top middle step on Mask 2 in Figure 3.7):

1. Six electrode pattern
2. Six electrode device (*without microchannel*)
3. Selectable microchannels (see Figure 3.8)
4. Large fluid inlet and outlet patterns
5. Small fluid inlet and outlet patterns

The design drawings for the mask designs were sent to Photo Sciences Corporation in Torrance, CA for production using their "fast track" program.

3.1.9.1 Selectable Microchannel Design. As mentioned in Section 3.1.7, the microchannel widths are selectable for both the four and six electrode designs. The selectable microchannel design was included for robustness. The ability to make a choice on

which microchannel width to use counteracts the effect of two undesirable contingencies. First, it was not clear at the beginning of the project which facilities, equipment and materials would be available for the fabrication. The selectable microchannel fabrication process requires a plasma ashing step not available at the AFIT cleanroom. Second, problems with cell flow on a prototype microdevice were anticipated. If a smaller or larger microchannel should be found to be necessary at a late stage of the project, it would be desirable to have a choice of channel widths on the existing masks to use in an attempt to fabricate a replacement.

In addition to those unknowns, there was another possibility that even if equipment became available to complete both fabrication processes, that there would be an excessive time burden for fabrication of the selectable channel devices. Having multiple designs on the mask made it possible to make a choice between designs based on the anticipated time it would take to fabricate.

The selectable microchannel design is more complicated and adds additional alignment, masking and etching steps along with necessary equipment to the fabrication process. The two electrode device is a simpler design and allows for a reduction of scope of the project if the proper time and equipment is not available. Figure 3.8 shows the location of the selectable microchannels on Mask 2. The microchannels on the mask are accompanied by a set of precise alignment marks to ensure that the channel pattern is applied where it is needed. There are separate alignment marks for each channel that match up in a unique way with alignment marks from the previous mask step.

In order to facilitate the design of the micro-fluidic device, the requirement list in Table 3.2 was compiled. The listing of the requirements is an example of the care taken during the design phase to lower the chances of serious fabrication issues. A well thought out plan reduced surprises and helped avoid costly design flaws. Table 3.2 is a representative list of requirements used during the mask design phase of the project. The table lists the design requirements for the microfluidic device designed for this thesis project. Listing the requirement's names, descriptions and reasons and checking them off once complete was critical to creating a well designed microchannel system. A similar list was used to plan the test setup.

Table 3.2 Design Requirements for Micro-fluidic Device

Number	Requirement	Description / Task	Reason
MCDR-01	Channel Length (Selectable Channels) - 190 μm	Check that lengths of selectable channels in the final design file are set to 190 μm	190 μm on mask but only 160 μm is usable, the rest will overlap and used for buffer for misalignment
MCDR-02	Channel Width (Fixed) - 12 μm	Check final design file to ensure fixed channel width is set to 12 μm	Based on cell sizing data collected
MCDR-03	Channel Width (Selectable) - 10 μm , 12 μm , 15 μm	Check final design file to ensure final selectable channel widths are: 10 μm , 12 μm , 15 μm	Different cell sizes require different channel size
MCDR-04	Electrode Width - 20 μm	Check final design file to ensure electrode widths are set to 20 μm	Standardize electrode width for simplicity
MCDR-05	Electrode Gap - 9 μm	Check final design file to ensure final electrode gap on all designs are: 9 μm	Fix electrode gap for simplicity of design
MCDR-06	Large Cover Slip Fluid Port Diameter - 7 mm	Check mask design drawings to ensure large fluid ports are 7 mm diameter	Fit to standard pipette inner diameter
MCDR-07	Total Device Dimensions - 41.2 mm \times 20 mm	Check overall device length in design file is 41.2 mm end to end and 20 mm across	
MCDR-08	Add Descriptive Text for Channel Size and Alignment Marks	Include text in mask design	Descriptive text that will help a user should be added
MCDR-09	Check Overlap of Alignment Marks	Ensure that alignment marks added to each feature line up correctly	Avoid misalignments

MCDR-10	Remove Any Spaces from File Name or Top Structure Name	Check that the file name & top structure name has no spaces	Requirement from Photo Sciences
MCDR-11	Comply with Minimum Feature Size	3 μm for straight lines; 5 μm for angular lines; 5 μm for squares	Smallest feature size requirement from Photo Sciences
MCDR-12	Check for Data File Inconsistencies	Data on data, self intersections, non-connected vertices	Contradictory data issues confuse the foundry
MCDR-13	Dimensions in Data File and Order Form Must Match	Ensure dimensions are in microns on final data file and microns is checked on the order form	Match units
MCDR-14	Channel Must be Continuous	Check all fluid channels for gaps between component shapes	Any blockages of the channel will render the chip useless
MCDR-15	Instance Alignment Marks	Make alignment marks an instance to allow changing width in design	Ease the implementation of alignment marks, ensure they are all the same
MCDR-16	Clear Rulers from Ledit File Before Exporting		Ensures ruler lines will not be mistakenly drawn by the mask foundry
MCDR-17	Adhere to Design Rules from Mask Provider (Photo Sciences)	Check final design against all provided design rules	Avoid problems related to foundry
MCDR-18	Final Data File is GDS, DXF or PG	Ensure output file format	Design rule from Photo Sciences
MCDR-19	Data Center (0, 0) Must Match Plate Center	Ensure data center matches desired plate center	Design rule from Photo Sciences
MCDR-20	No Data Within 6.35 mm from Edge of Plate	Check drawing to ensure no features are beyond limit	Design rule from Photo Sciences
MCDR-21	Design File Size Can Not Exceed 150 MB	Check file size	Design rule from Photo Sciences

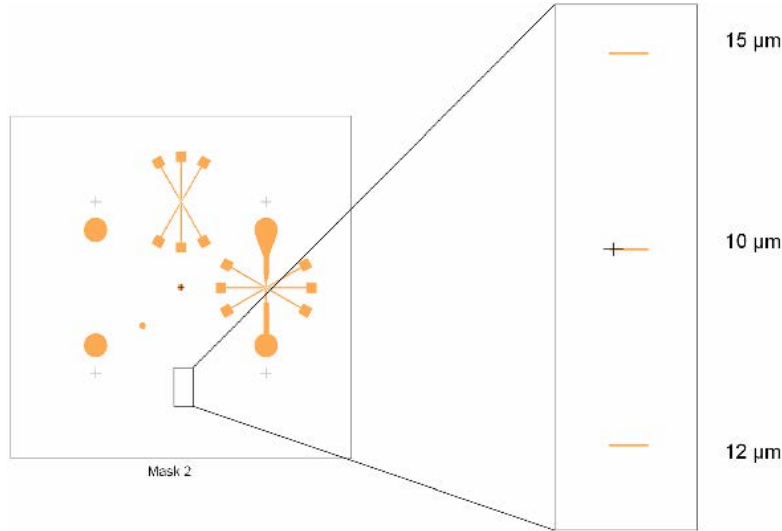


Figure 3.8 There are three separate microchannels to choose from when using the four and six electrode microdevice design. The pattern for the selectable microchannels is included on the middle bottom part of Mask 2. They are barely visible to the naked eye.

3.1.9.2 Mask Feature Placement and Alignment Planning. In order to conserve space and to lower the production cost, four separate mask steps were included on each mask. Planning and simulation was necessary to ensure the usefulness of the shared mask. Figure 3.9 shows the guideline tool used to lay out the features on the masks. This design tool allowed the visualization of all areas where adjacent mask features unintentionally appear on the two inch wafer. By rotating a design drawing of a complete device and placing it on top of the features in each circle, it can be demonstrated that a device can be fabricated using these steps without overlap of features.

The electrode design was modified after running such a simulation. The original device design involved 'L' shaped electrodes. The pads of the electrodes with the old design tended to interfere with the features on the adjacent mask steps. Making the electrodes perpendicular plus and minus 29° to the channel reduced interference considerably. Further discussion of the early design work is included in Section 3.1.15.

3.1.10 Materials. The choice of materials is important in a micro-fluidic design to ensure biocompatibility, mechanical strength, durability in contact with water, electrical and

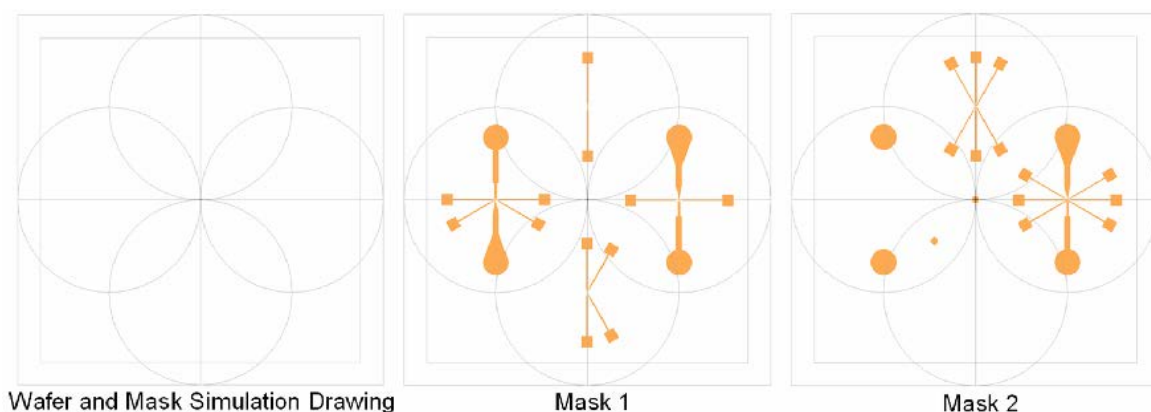


Figure 3.9 Guideline drawings were used to simulate the overlap of the mask steps. The guideline simulation drawings are shown on the left. The outer square marks the border of the 4 inch mask plate. The inner square marks the allowable design space mandated by the mask makers. The circles are 2 inches in diameter and show where there is overlap of the mask steps. The middle and right picture show how the final masks fit inside the guidelines.

Table 3.3 Mechanical and Electrical Properties of Pyrex Substrate

Property	Units	Value
Density	<i>g/cc</i>	2.23
Hardness	Knoop	4.18
Young's Modulus	GPa	62.75
Log Volume Resistivity	Ω cm	8×10^{10}
Dielectric Constant (20 °C, 1 MHz)	–	4.6

thermal properties etc. The following information was compiled using available technical documentation [7, 8, 17, 30, 31].

3.1.10.1 Pyrex Substrate. The decision was made to use a Pyrex 7740 glass substrate based on the requirement that the microchannel be visible using the predominately inverted microscopes in the biological laboratories at AFRL/HE (where the cell work was carried out). Pyrex is a borosilicate float glass with low thermal expansion properties manufactured by Corning. Table 3.3 is a list of relevant material properties and was compiled using information on the Corning Corporation and Inasco Corporation websites. The table lists mechanical and electrical properties of the Pyrex wafers used as the substrate for the microdevice. Pyrex is very well suited as the substrate because it is mechanically durable, optically transparent and has a high resistivity.

3.1.10.2 Photoresists. Several different photoresists are used in the various patterning steps called for in the design. The reasons for choosing the photoresist that were used and descriptions of their properties are included below.

Negative Masks Effected Resist Choices. The most critical photoresist is SU-8 Formulation Number 5 (SU-8 5) which is used as a permanent structural layer to form the channel walls. SU-8 is a negative resist therefore negative image masks were designed to pattern the channel. All of the masking steps were designed to pattern negative resists only.

SU-8 Formulation Number 5. As mentioned above, SU-8 5 was chosen as the resist to use for the structural layer in the microchannel device. SU-8 is a class of photoresists manufactured by Micro Chem Corporation in Newton, MA. There are several different formulations numbered 2-25. The formulation numbers indicate the nominal thickness in microns that will be achieved using a standard spinner RPM value of 3000. So the nominal thickness for SU-8 5 is 5 μm at 3000 RPM. SU-8 is very well suited as a permanent layer in micro-fluidics. SU-8 has been found to be biocompatible, it is structurally sound and will not breakdown under normal use with water and biological agents. SU-8 is an epoxy based photoresist that forms an optically transparent structurally sound layer which is very resistant to chemicals and temperature fluctuations [31].

NR9-1000PY. NR9-1000PY is made by Futurrex Corporation in Trenton New Jersey. It is a negative resist specially formulated for use with the metal liftoff technique of patterning metal on microdevices. This resist was obtained from the AFRL cleanroom. The intended use for this resist was patterning Titanium / Gold seed layer electrodes using metal liftoff. This process was successfully completed using the initial design however it was not used for the final design. NR9 was also a candidate for use during the cover slip etching process.

SF-19. SF-19 is a thick polydimethylglutarimide (PMGI) positive resist typically used as a sacrificial layer or the bottom layer in a liftoff process. It does not react with typical solvents used in most resists so it will not mix if used as the lower

layer in a bilayer process. It can be used for deep UV multiple exposure and development applications. SF-19 can form features as tall as 19 μm .

AZ5214E. AZ5214E Image Reversal Resist is a versatile resist that can be used for either positive or negative patterning. If only one exposure step is used, AZ5214E behaves like a positive resist because the areas exposed to UV are developed away using regular positive resist developer. For use with negative image patterning, a post exposure bake (PEB) is added after the first exposure step and then a flood exposure is performed which exposes the entire resist surface. The PEB is key to the image reversal because it causes cross-linking in the areas that were exposed during the first (patterned) exposure. The cross-linking in the exposed area makes that area resistant to the resist developer. The flood exposure exposes the previously unexposed area and thus allows it to be developed away with the positive resist developer [5].

3.1.11 Fabrication Steps. Other aspects that have to be thoroughly thought out during microdevice design are the fabrication steps that will be necessary. The focus should be on reducing the number of steps and minimizing the time and resources required to fabricate. The other considerations effecting the choice of fabrication steps are the available resources. For example, if there is no access to a capability to electroplate, the design should avoid electroplating and seek alternatives for metal deposition. The designs chosen for this project were influenced directly by the capabilities of the AFIT and AFRL cleanrooms. The fabrication steps envisioned in the design phase were checked against their capabilities. Based on this analysis, the design was ostensibly found to be possible.

The equipment of use for this project in the AFIT cleanroom are the following: Karl Suss MJB3 Contact Mask Aligner, Alpha Step IQ profilometer, optical microscope with camera, resist spinning and baking equipment and a metal evaporation system. At the time of the initial design work it was assumed that the necessary equipment and materials at the AFRL cleanroom such as electroplating, plasma etching and photoresists would all become available to process the steps that require them. Figure 3.10 is the final processing map for the two electrode design. A step by step account of the results of the fabrication process is detailed in Chapter IV.

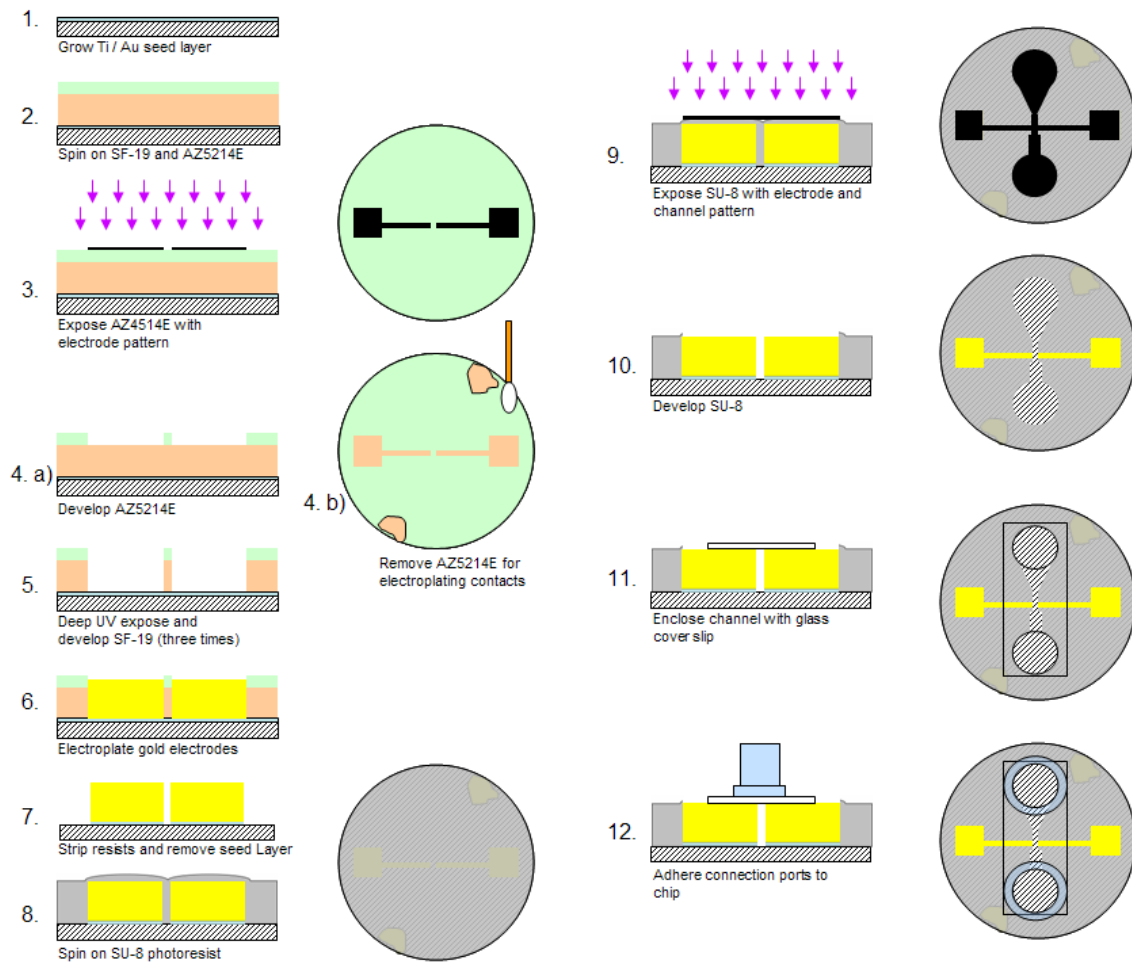


Figure 3.10 This figure maps out twelve main fabrication steps. Step 1. A Ti / Au seed layer is evaporated onto the Pyrex wafer. Step 2. SF-19 and AZ5214E resists are spun on. Step 3. The AZ5214E is exposed using the two electrode pattern. Step 4. The AZ5214E is developed. Now the electrode pattern reaches down to the SF-19 layer. A cotton swab is used to remove AZ5214E in the two areas where the electroplating contacts need to touch the seed layer. Step 5. Three to five consecutive deep UV exposures and SF-19 developments. This removes the patterned photoresist completely down to the seed layer. Step 6. The gold electrodes are electroplated up to the height of the photoresist walls. Step 7. The stripping of the resists and removal of the seed layer. Step 8. The wafer is conformally coated with SU-8 up to the same height as the electrodes. Step 9. The SU-8 is exposed with the channel plus electrode pattern. Step 10. SU-8 is developed. SU-8 is completely removed from the channel and the electrodes. Step 11. The channel is capped with a glass cover slip. Step 12. Fluid ports are bonded on with UV curable adhesive.

The process maps for fabrication of the four and six electrode designs are identical to one another but different from the two electrode fabrication process because the latter includes some extra steps. For the four and six electrode device designs, a series of steps need to be inserted between step 10 and step 11 in Figure 3.10. The difference actually begins in step 9 where the four and six electrode second masking step does not clear the micro channel. Instead, the channel must be selected and plasma etched into the SU-8 between the electrodes. The new step 10 would be coating the wafer with a negative photoresist like AZ5214E or NR9. Next step 11 would be to carefully align the microchannel pattern on Mask 2 in between the electrodes and to connect the inlet channel with the outlet channel and then expose with UV. After exposing and developing the resist, step 13 would be to plasma etch the wafer to remove the SU-8 in the microchannel while leaving all of the rest of the SU-8 intact. At that point, the process returns to step 11 on Figure 3.10 for application of the cover slip and the fluid ports.

3.1.12 Cover Slips. Most of the device can be constructed using microelectronic style photolithography and chemical based processing steps in the cleanroom. After the fabrication of the channel is complete in the cleanroom, the channel must be closed off on the top to make a water tight three dimensional tube which will confine movement of the cells during use. Although easily overlooked as perhaps less important, the design of reliable interconnections to and from microdevices is one of the most challenging areas in micro-fluidics. The following sections on cover slip design show how the design evolved as more information became available and as the significance of a good design in this area became more apparent.

3.1.12.1 Early Cover Slip Design. The first cover slip envisioned for the design was a separate 150 to 200 μm thick 2 inch diameter Pyrex wafer. Two large (7 mm) inlet and outlet holes were to be etched completely through using hydrofluoric acid. Then the wafer with the large fluid holes would be cleaved on the right and left side to around a 1 inch width. Cutting the cover slip on the side provides access to the electrodes. The openings to the channel on the SU-8 masks were set at 7 mm. The dimensions of the cover slip through holes correspond to the inner diameter of standard glass tubing used in laboratories.

3.1.12.2 Later Cover Slip Design. The later cover slip design was based on standard number 1 thickness, 22 mm X 30 mm glass slide cover slips (Fisher Scientific Catalog No. 12-548-5A) instead of thin Pyrex wafers. The design change was due to the realization that the pressure necessary to drive fluid flow through a channel increases with channel length. Further discussion on the cover slip design change is included in Section 4.2.1. The original design called for a 41.2 mm long device with a covered channel length of 27.2 mm. Using the standard cover slips reduced the covered channel length down to around 7.2 mm. The final mask designs included patterns both for masking the large original etch holes and for smaller holes positioned about 20 mm apart.

One last redesign occurred during the fabrication process. Lack of materials hampered efforts to etch through the cover slip to form the through holes. Instead, the holes were drilled through the cover slip using a diamond bit on a Dremel 400 XPR rotary tool set to the lowest RPM setting. Through holes measured approximately 2 mm in diameter and were approximately 7 mm apart. The cover slips were then cleaved into rectangles 18 mm X 8 mm; which is much smaller than the full cover slip. The reduction in size helped to control the UV curable adhesive as discussed in Section 4.2.1.

3.1.13 Fluid Ports. Raised fluid ports were deemed to be necessary from the beginning of the design process. The fluid ports serve as a protection against the effects of evaporation and as interconnections to the aspiration system. Extremely small quantities of water such as those necessary to fill the microchannel evaporate very quickly. The evaporation can change the properties of the fluid inside the channel by altering the concentrations of suspended particles. The ratio of water loss due to evaporation vs. total water is reduced drastically with the addition of the fluid ports. The manual aspiration system described in Section 3.1.14 connects to the microdevice at the fluid port. The most convenient fitting that could be easily fabricated was a standard 7 mm outer diameter glass tube cut to a length of approximately 6 mm. The glass fluid ports are adhered to the cover slip providing access to the through holes and to the channel. The fluid ports on the top restricted the ability to use standard light microscopes to view the microchannel. Since the device was constructed on the Pyrex wafer, the microchannel could still be viewed using inverted light microscopes.

3.1.14 Aspiration System. The aspiration system design evolved during the course of the project but always remained quite simple. The job of the aspiration system is to create a pressure differential across the fluid ports in order to drive fluid flow in a desired direction at a desired flow rate. The first design idea was a motorized pipettor to be connected to the outlet port via 1/4 inch inner diameter PVC tubing. The final design for the manual aspiration system was a 10cc syringe connected to the input port. Air pressure is applied to the fluid port by compressing the air with the syringe plunger (typically 3-5 cc's).

3.1.15 Design Evolution. This section reviews the parts of the design that underwent large evolutions during the course of the project. The section is meant to call attention to some of the hidden design issues that became more clear after working on the project. Some design requirements remained constant throughout the entire project and others evolved based on new information.

3.1.15.1 Early Design Iteration. There are many differences between the final design and the first designs produced for this project. The first microdevice design concept envisioned the use of a rectangular glass substrate with L shaped electrodes (see Figure 3.11). This design used four measurement electrodes for use with a four point impedance measurement instrument. A simpler two electrode configuration is shown on the preliminary mask designs in Figure 3.12. Figure 3.12 hints at the difficulty of designing the shared mask layout using the L shaped electrode design. The electrode height for the devices shown in these two figures was designed to be at seed layer level. The SU-8 is very flat when the cover slip is applied over the microchannel. The cover slip has the same width and only a slightly smaller length than the substrate. Figure 3.12 contains a concept of allowing selectable micro electrode widths and gaps.

Some aspects of the final design are also visible in this preliminary work. SU-8 is used as the structural layer in the device drawn in Figure 3.11. A tapered channel, 7 mm fluid ports, and selectable microchannels are all seen in Figure 3.12.

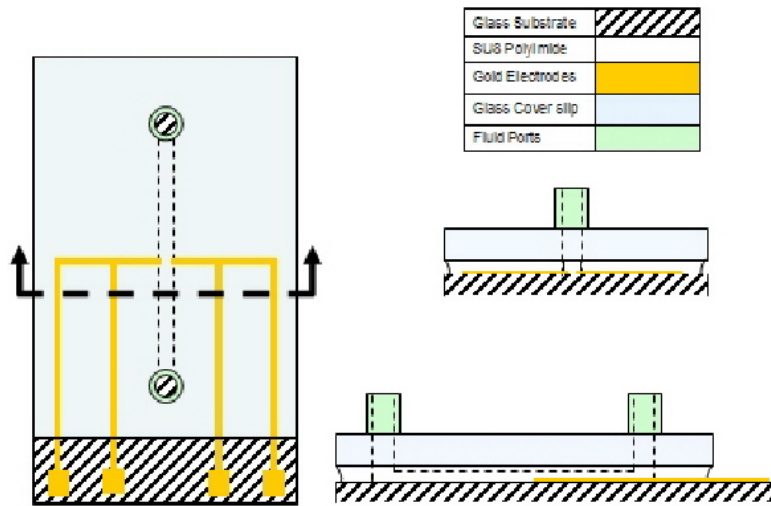


Figure 3.11 This figure illustrates a concept formed after the initial iterations of design. A square substrate was envisioned (possibly a glass slide). The original design was a four electrode design for better accuracy. The electrode traces are patterned in the 1000 Angstrom seed layers and do not match the channel height. SU-8 is used for the channel layer just as in the later designs.

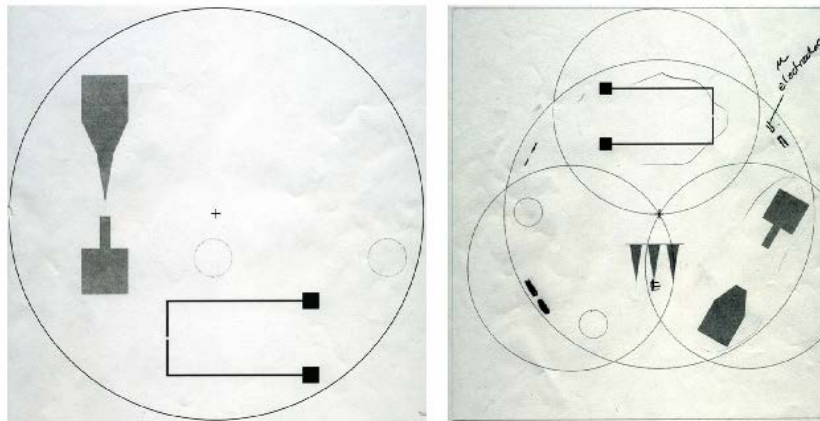


Figure 3.12 This figure shows two separate early mask designs. The largest circle representing the viewable area on the mask aligner is shown in both pictures and is of particular importance. Patterns on the mask all need to be viewable through the large circle which can translate to the left or right about 1/2 inch. Features in the design on the left are offset from one another by 120 degrees which proves cumbersome for alignment purposes. The mask design on the right represents the next design iteration in which all components are offset by 90 degrees.

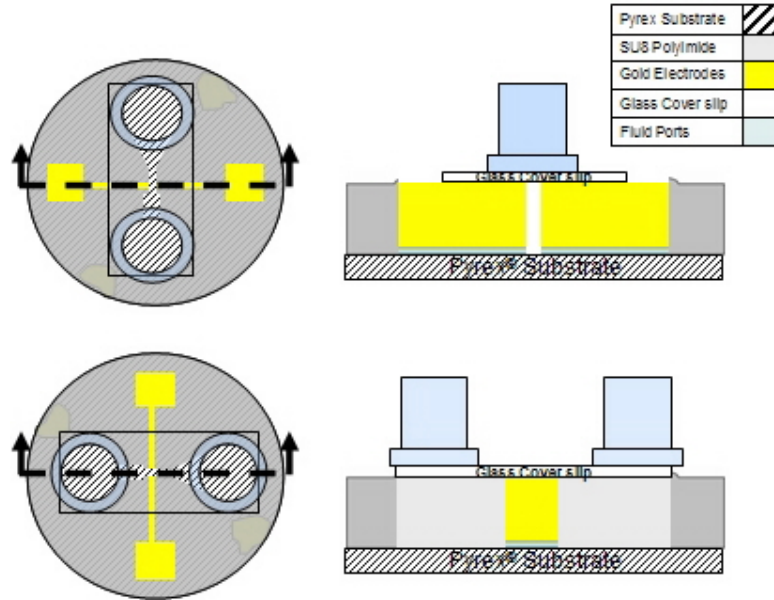


Figure 3.13 This cartoon shows the final two electrode micro device design. The drawing is not to scale but illustrates the major features. The main features of this design are: electroplated gold contacts at the same height as the SU-8 channel, round Pyrex substrate and the two electrodes perpendicular with the channel.

3.1.15.2 Final Device Design Iteration.

The final designs are for three separate devices. The class of devices that were fabricated for this project were all the two electrode design like the one shown in Figure 3.13. Further discussion about the motivation for the design changes during fabrication are given throughout Chapter IV. The two electrode design that was implemented featured electroplated gold electrodes and an SU-8 structural channel layer formed after the electroplating. The SU-8 layer was designed to be applied after the electroplating. The order of the SU-8 application effected the flatness of the SU-8 layer that the cover slip was bonded to. The application of the conformal layer of SU-8 after the electroplating created the effect of a gentle slope in the SU-8 profile going from low, away from the electrodes, up to high, near the electrode / SU-8 border. The cover slip in the final design is proportionally much smaller than the substrate to enable the cover slip bonding method used.

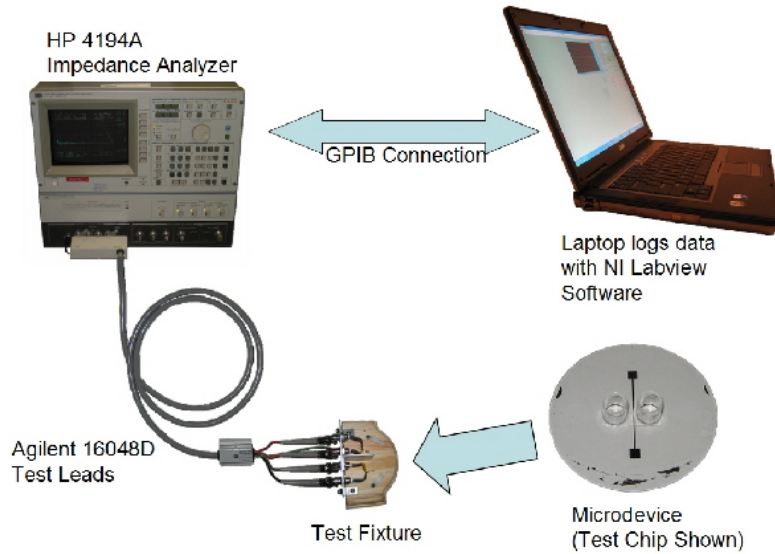


Figure 3.14 This diagram illustrates the connections between the impedance analyzer and both the test fixture and microdevice. The HP4194a impedance analyzer is connected to the test fixture for reading impedance data and also connected to the laptop computer for logging impedance data for analysis.

3.2 Testing Equipment Configuration

The testing setup for this thesis consisted of an HP4194a Impedance Analyzer made by Agilent Technologies taking measurements from a user fabricated test fixture connected to the microchannel device. The impedance analyzer was controlled remotely using a General Purpose Interface Bus (GPIB) connection to a laptop computer that was running a customized Labview program that logged impedance data. Figure 3.14 is the block diagram describing the interaction between testing equipment.

3.2.1 Impedance Analyzer. The HP4194A impedance analyzer has a frequency sweep range from 200 Hz to 15 MHz with a one meter extension cable in place. If the test fixture is moved directly to the impedance measurement terminals, the range is extended to 40 MHz. The decision was made to fabricate the test fixture and use a one meter cable. The impedance analyzer can take precise impedance measurements at up to 401 points along a sweep. It can be interfaced to a laptop computer via the GPIB.

A one meter cable was made from Agilent supplied parts and used to connect to the test fixture. A test fixture was designed as an interface between the shielded coaxial measurement cables and the microdevice. The test fixture consisted of a (wooden) base,

L brackets connecting to an Agilent manufactured test fixture interface plate, four 5 cm 20 AWG wires connecting to the interface plate, gold contacts made using Radioshack Goldseries Deluxe Flat-Pin Connectors and two plastic spring clips to hold the gold contacts to the electrodes on the microdevice.

3.2.2 Instrument Control. National Instruments Labview was used to implement a program to control the HP4194A and to log impedance data. The Labview program (called a VI or a virtual instrument) was based on sample code available at the National Instruments web site. The sample code was written by Brian Beal and posted on the National Instruments Developer Zone web site. The sample code was modified for this project.

The final Labview VI performs the following actions:

1. Run an open and short calibration sequence
2. Run an impedance measurement sweep over a user selectable frequency range
3. Logs 401 data points for the entire sweep
4. Saves the impedance magnitude and phase data in separate space delimited files

3.3 Summary

This chapter described the issues faced and overcome during the design phase of this project. Three separate microdevices were designed to meet the overall requirement of a working microdevice for impedance spectroscopy. Initial planning and design work focused on battling the unknown. Options and variety were made a part of the designs to increase the ability to deal with unforeseen challenges in the fabrication process. The design evolved along the way based on information learned while attempting fabrication.

An impedance measurement test station was planned. The test station consists of an impedance analyzer, extension cables, a test fixture and the impedance microdevice. The test station is controlled remotely from a laptop computer running National Instruments Labview. The robust set of designs created during the planning and design phase are essential to fabrication success.

IV. Fabrication and Testing Results and Analysis

4.1 Introduction

One of the three designs discussed in Chapter III (the two electrode design) was fabricated and functionality verified. This chapter describes all of the fabrication processing details for the microdevice as well as impedance data collection and analysis. The fully functional microdevice is shown in Figures 4.1 and 4.2. Masks were produced by Photo Sciences Corporations based on the mask designs discussed in Chapter III. Figure 4.3 shows the completed masks used during the fabrication steps.

Impedance measurements were taken using the microdevice and the test setup discussed in Section 3.2. Two devices were used to record impedance measurements: test device MC-01 and final device MC-05. Seven separate data sets were recorded using the final device (MC-05): Air, Phosphate Buffered Saline Solution (PBS), Deionized Water (DIW), Live Cell Run 1, Live Cell Run 2, Dead Cell Run 1 and Dead Cell Run 2. Each data set contains about 20 impedance sweeps. The maximum frequency range was used to make impedance measurements on MC-05. Impedance was recorded at 401 points along a frequency sweep of 1 kHz to 15 MHz on MC-05. On the test device MC-01, impedance data was collected using a frequency sweep from 1 kHz to 3.7 MHz and only 100 data points were recorded due to an error in the Labview program. Magnitude and phase of all the separate sweeps performed using microchannel MC-05 and MC-01 were saved to a laptop hard drive. Further discussion and analysis of the recorded data is included in Section 4.3.

There are two main sections in this chapter: Micro Device Fabrication Processes and Microdevice Testing. The section on fabrication discusses the step by step process used to fabricate the device. A high level of detail is included to allow readers to more easily reproduce this work and to emphasize areas where planning and design work can help avoid fabrication problems of similar devices. The testing section describes the facilities, equipment and the testing process used to make impedance measurements. This section also displays data recorded from the measurements, along with various analyses performed.

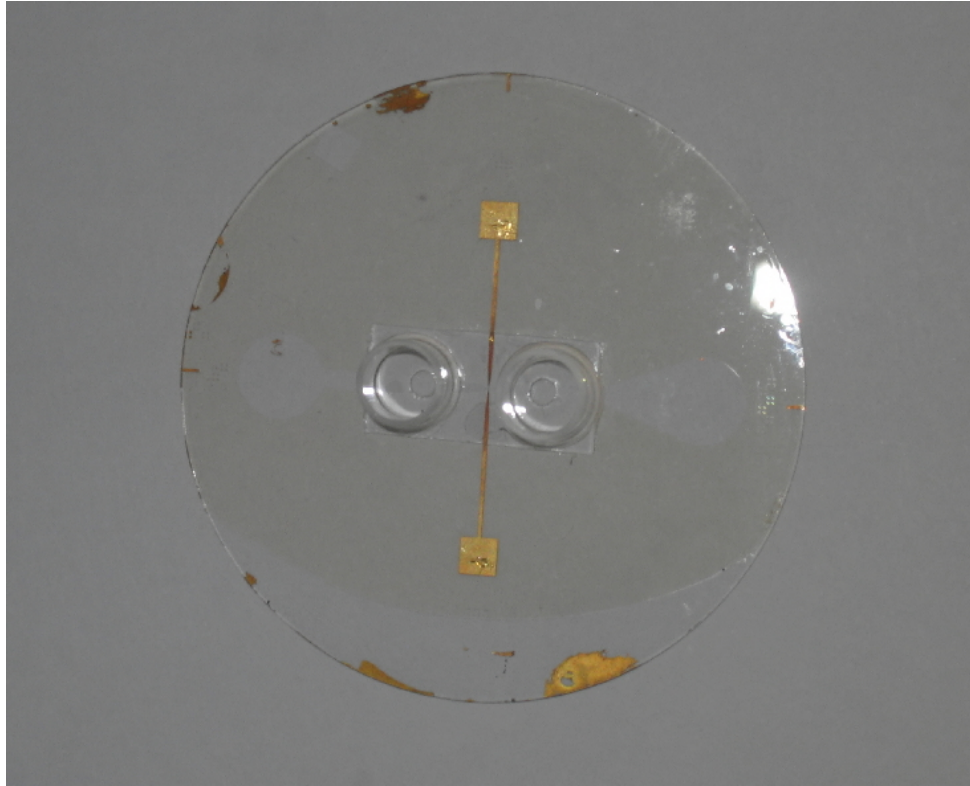


Figure 4.1 This figure shows the top view of the microdevice fabricated during this effort. It consists of a microchannel made from SU-8 that runs between two electroplated gold microelectrodes. The device designation number for the device is MC-05.

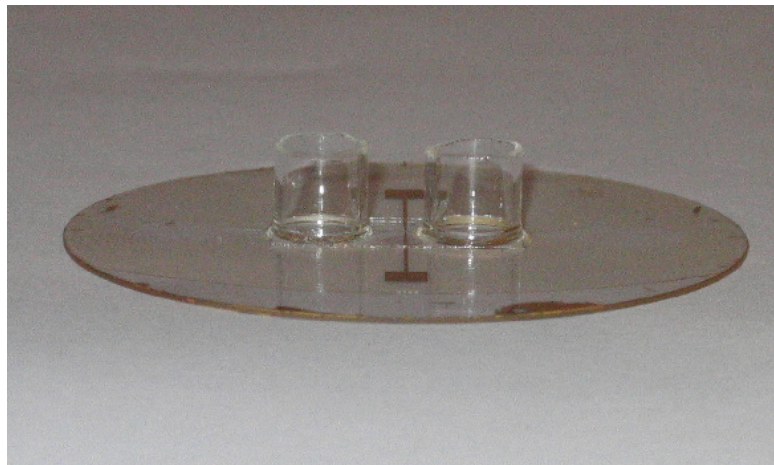


Figure 4.2 This figure shows device MC-05 from the side. The profile of the glass fluid ports are visible in this photograph.

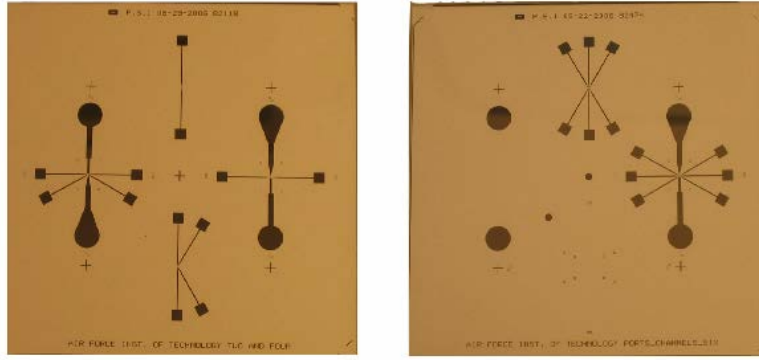


Figure 4.3 This figure shows the masks produced by Photo Sciences Corporation based on the designs discussed in Chapter III. The masks are soda lime glass and the patterns are in chrome.

4.2 Micro Device Fabrication Process

There was a step by step photolithographic fabrication process which included metal deposition, photoresist, application, patterning and removal, metal etching, O₂ plasma ashing, alignments and wafer cleaning steps. Although the microfabrication portion of the design was relatively complete early on, there were numerous areas encountered during the fabrication process which required careful attention to complete. Experience gained during the course of the microdevice fabrication caused the designs to be modified. Process steps were refined to a much higher level of detail during the fabrication time period than they were in the design phase. Several unplanned problem areas are discussed presently along with their causes and solutions.

In addition to the microelectronics based cleanroom work, there were efforts to build cover slips and fluid ports using additional processes. The fabrication and bonding of the ports and cover slips were a larger challenge than anticipated in the early design phase. The work done, that ultimately led to a successful device, is described in detail. Testing of the device functionality and collection of cell impedance data is discussed in the final section of this chapter.

4.2.1 Step by Step Micro Device Fabrication. This section describes the processing steps taken to build the microchannel device. The work done during each step shown in Figure 4.4 which repeats Figure 3.10 is described. As mentioned in Section 3.1.15, the design evolved throughout the fabrication. In some cases, fabrication steps were attempted

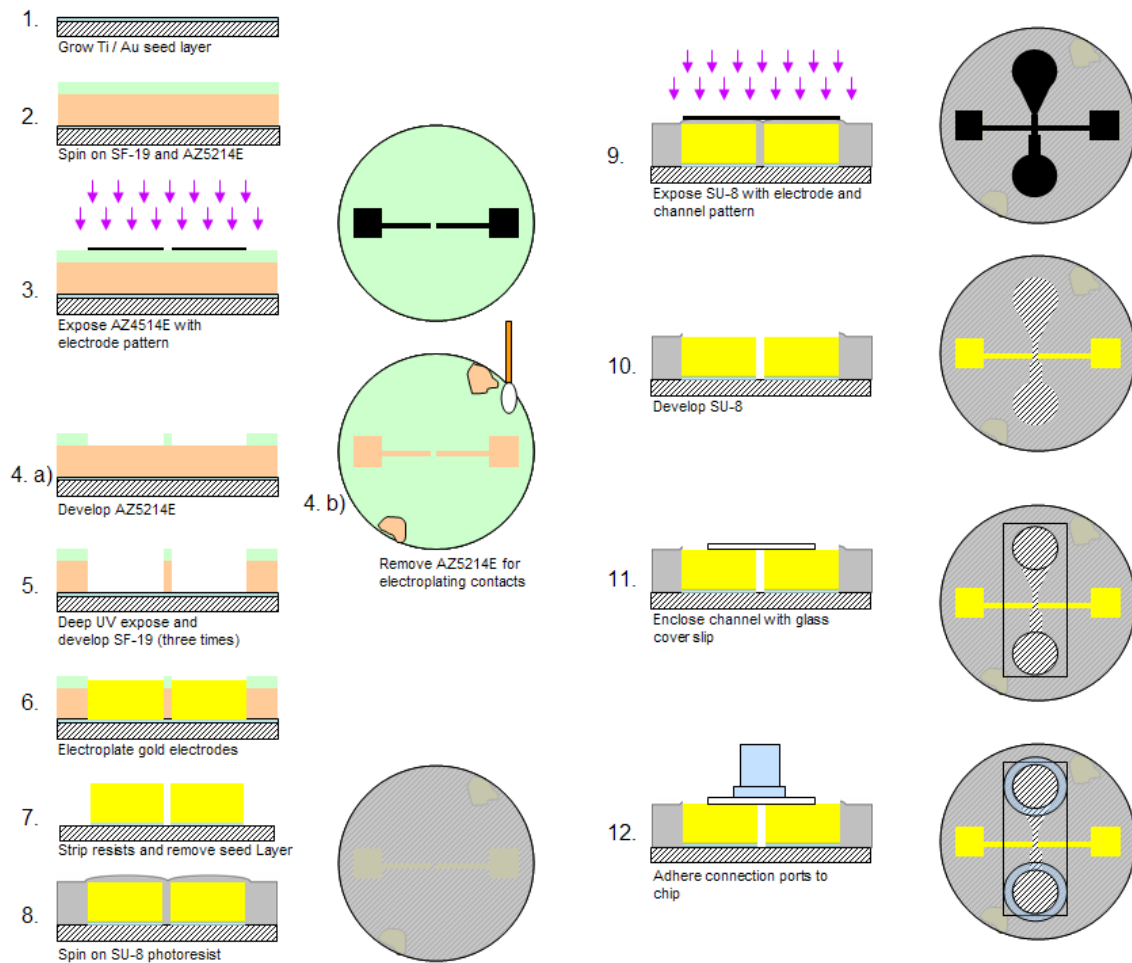


Figure 4.4 This figure maps out twelve main fabrication steps. Step 1. A Ti / Au seed layer is evaporated onto the Pyrex wafer. Step 2. SF-19 and AZ5214E resists are spun on. Step 3. The AZ5214E is exposed using the two electrode pattern. Step 4. The AZ5214E is developed. Now the electrode pattern reaches down to the SF-19 layer. A cotton swab is used to remove AZ5214E in the two areas where the electroplating contacts need to touch the seed layer. Step 5. Three to five consecutive deep UV exposures and SF-19 developments. This removes the patterned photoresist completely down to the seed layer. Step 6. The gold electrodes are electroplated up to the height of the photoresist walls. Step 7. The stripping of the resists and removal of the seed layer. Step 8. The wafer is conformally coated with SU-8 up to the same height as the electrodes. Step 9. The SU-8 is exposed with the channel plus electrode pattern. Step 10. SU-8 is developed. SU-8 is completely removed from the channel and the electrodes. Step 11. The channel is capped with a glass cover slip. Step 12. Fluid ports are bonded on with UV curable adhesive.

using more than one method. Design changes were largely due to equipment constraints and processing knowledge gained which required modification of the specific methods used to achieve a goal. When steps with more than one method are discussed in this section, the processing steps according to the early design iterations will be described along with the processing steps performed for the final designs.

Step 1: (Initial Design) Electrode Seed Layer Deposition

Processing for this step changed significantly during the project so there are more than one methods described for this step. The masks were designed with the goal of creating electroplated electrodes at the same height as the microchannel walls made out of SU-8. In order to electroplate, a metal seed layer must be used as a starting point for the reduction reaction that takes place in the electroplating bath.

Two methods of electroplating the electrodes were attempted. A description of both strategies are provided. The first appears here, and the second under the step labeled "Step 1 (Final Design) Electrode seed Layer Deposition". The latter corresponds to the final process flow chart shown in Figure 4.4.

The first seed-layer design used a metal liftoff method with SU-8 to form a 1000 Å thick set of electrodes patterned directly on the seed layer. It was assumed that electrical contact with the electroplating bench could be made to the electrodes patterned into the seed layer. This concept would allow the electrodes to be grown level with an SU-8 channel layer. A bilayer SU-8 liftoff process using LOR-3A and SU-8 was developed by Major Glen Kading for use in another microfabrication process and is shown in Table 4.1. The process is intended for use in patterning Ti / Au seed layer metal. The Ti / Au metal deposition time is dependant on the electron beam evaporator's parameters. This process was used to pattern the electrodes.

SU-8 is not particularly well suited to the liftoff procedure. SU-8 is an epoxy based resist and it is quite difficult to completely remove from a wafer once it has been exposed and crosslinked after the post exposure bake. The bilayer process is necessary for the liftoff procedure because SU-8 tends to form nearly vertical sidewalls on patterned features. An undercut is desirable in metal liftoff because it tends to better separate patterned metal and reduces problems such as metal stringers left over after metal removal. Figure 4.5 shows

Table 4.1 SU-8 Metal Liftoff Process Steps

	Step	Process	Time
1.	Clean Wafer	Clean on spinner using acetone and isopropyl alcohol	2 min
2.	Coat Wafer with LOR-3A	Spin - 3000 RPM	45 sec
3.	Soft Bake LOR-3A	Hotplate 150 °C	5 min
4.	Coat Wafer with SU-8 5	Spin - 3000 RPM	30 sec
5.	Soft Bake SU-8 5	Two step bake on hotplate: 65 °C, then 110 °C	4 min, then 4 min
6.	Expose SU-8 5	220 mJ/cm ² 365 nm UV	25 sec
7.	Post Exposure Bake SU-8 5	Repeat step 5	4 min, then 4 min
8.	Develop SU-8 5	Use SU-8 developer from Micro Chem	2 min
9.	Create LOR-3A Undercut	Use LDD-26W developer	90 sec
10.	Evaporate Ti Layer	250 Å Ti	NA
11.	Evaporate Au Layer	750 Å Au	NA
12.	Perform Metal Liftoff Procedure	Use 1165 stripper to remove SU-8 and LOR-3A	20 min
13.	Remove Residual Resist	Use acetone squirt bottle and acetone bath	time varies
14.	Rinse	Isopropyl alcohol rinse and N ₂ dry	15 sec



Figure 4.5 This figure shows the results of a Titanium and Gold seed layer patterned with an SU-8 liftoff process. Rough edges around all of the electrode parts can be seen. The rough edges widen the electrode gap by approximately half of a micron.

the results of the SU-8 liftoff for patterning the microelectrodes. The poor line quality with rough edges around the patterns changes the design dimensions. The rough liftoff pattern may be a result of the mechanical scrubbing necessary to remove the residual SU-8. In order to get better quality results, other methods of seed layer patterning were sought.

An alternative procedure for liftoff used NR9-1000PY photoresist from Futurrex Corporation. This negative resist is formulated especially for metal liftoff. The undercut can be controlled by varying the exposure time. A longer exposure leaves a smaller undercut and a shorter time produces a larger undercut. After using a 3000 RPM spin rate on the AFIT cleanroom spinner, the NR9 resist thickness was measured using a Alpha Step IQ profilometer to be 1.1 μm in height. Table 4.2 lists the NR9 liftoff process steps used. Metallization time is dependent on sputtering system parameters. The process described in Table 4.2 is much simpler and takes less time than the SU-8 bilayer process described in Table 4.1 because it uses only one photoresist and the processing step times are shorter. The other advantage to NR9 over SU-8 in this application is that NR9 can be removed simply with acetone and no mechanical scrubbing is necessary.

Several attempts were required to determine processing parameters such as bake times and exposure and development times to produce a quality pattern in all the resists used. Early attempts at using NR9 in the AFIT cleanroom were unsuccessful. Approximately

Table 4.2 NR9-1000PY Metal Liftoff Process Steps

	Step	Process	Time
1.	Spin Coat Wafer	Spin at 3000 RPM	45 sec
2.	Soft-bake	Hotplate at 150 °C	4 min
3.	Expose	Rough align pattern and expose on MJB3 aligner	5 sec
4.	Post Exposure Bake	Hotplate at 110 °C	2 min
5.	Develop	Use RD6 resist developer	10 sec
6.	Rinse and Dry	Rinse in DIW and dry with N ₂	1 min
7.	Evaporate Ti Layer	250 Å Titanium	NA
8.	Evaporate Au Layer	750 Å Gold	NA
9.	Perform Metal Liftoff	Use acetone bath and acetone bottle to dissolve NR9	3 min
10.	Rinse	Rinse in DIW	2 min

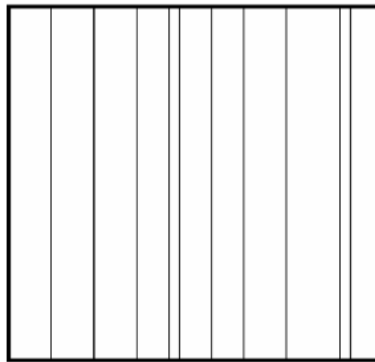


Figure 4.6 This figure shows the anomalous patterns that appeared on the majority of 50 test samples for NR9.

thirty test samples made from cleaved microscope slides were used for testing the patterning ability of NR9. Only about five test samples made useful patterns. The most common outcome when developing on the test samples was a line pattern (see Figure 4.6) which appeared over the mask pattern on the samples. Line patterns even appeared on the sample where the mask should have blocked the exposure. The initial guess about why NR9 did not develop properly is that the NR9 was being exposed when UV light was penetrating the glass wafer and bouncing back off the stainless steel chuck in the mask aligner to the underside of the photoresist. This hypothesis based on the patterns appearing as interference lines or a diffraction pattern. To counteract the diffraction, a UV absorbent pad was placed between the slides and the chuck in an attempt to diminish reflection.

Help from an experienced technician at AFRL was sought and processing of NR9 at the AFRL cleanroom went more smoothly. The diffraction theory was ruled out because

the contact mask aligner used in the AFRL cleanroom was not equipped with a dark pad and no lines developed. It was reported by members of the AFRL cleanroom staff that NR9 tended to be extremely sensitive to bake temperatures and humidity in the cleanroom. Both of the possibilities are quite plausible because bake times in the early processing were not strictly monitored and because there was a chronic water leak in the AFIT cleanroom ceiling which raised the humidity to critical levels. The humidity sensor's alarm sounded during processing on several occasions. Similar processing steps were used at the AFRL lab and the AFIT lab for NR9 processing with the exception that more attention was paid to adhering to the correct bake times.

With help from AFRL, a set of four wafers with electrode patterns in the seed layer were produced. First, four new Pyrex 7740 two inch diameter wafers were cleaned using acetone spray, acetone bottle and isopropyl alcohol bottle for approximately 15 seconds each. After cleaning, the wafers were dried with N₂ gas and placed on a 110 °C hotplate for a dehydration bake. Each wafer was processed according to the steps listed in Table 4.2. NR9-1000PY was patterned with the electrode pattern and then 250 Å of Ti and 750 Å of Au were evaporated over the patterned wafer. Next acetone was used to perform a liftoff procedure which removed all metal that was not deposited directly onto the glass. The liftoff patterning with NR9 made very clean lines and was overall a much better choice than the SU8 liftoff procedure. Four patterned wafers were produced during this step (MC-01, MC-02, MC-03 and MC-04). The MC designator uniquely identified the project's wafers (MC stands for microchannel).

After patterning the seed layer, equipment for electroplating was evaluated. It was determined that the electrodes could not be electroplated from the pattern in the seed layer only. A new batch of chips with a seed layer on the whole wafer was necessary. In order to electroplate, electrical contact must be made to the item being plated. The item being plated acts as the cathode in an electrochemical cell. The metal contacts need to make electrical contact to the gold seed layer for electroplating to occur.

The electroplating contact wires on the electroplating bench could not make contact with the electrode contact pads originally patterned onto the wafer. Figure 4.7 shows the board with the metal contacts used with the electroplating bath. There were also



Figure 4.7 This figure shows the contact board used to hold 2 inch wafers and to connect to the seed layers. The two metal contacts shown are held in contact with the seed layer by spring force.

some concerns by the AFRL team that the electroplating system could not be configured to metalize on the electrode pattern only because the current density would be too high. A redesign of the processing was necessary to address these issues.

Step 1: (Final Design) Electrode Seed Layer Deposition

The second and final design iteration for creating electroplated electrodes uses a seed layer over the entire wafer. Four new clean Pyrex wafers were used during this process. The designators of the wafers used in this sequence are: MC-05, MC-06, MC-07 and MC-08. Each wafer was cleaned with acetone and isopropyl alcohol then dried with N_2 . Next they were O_2 plasma etched to remove any residue on the surface before the seed layer metallization step. Finally, 250 Å of Ti and 750 Å Au were deposited over the entire surface of the wafers using sputtering.

Step 2: Spin Coat the Wafer with SF-19 and AZ5214E

A bilayer photoresist mold was created using SF-19 polyimide from Micro Chem and AZ5214E from Clariant. The SF-19 layer was 5-7 μm in height and the AZ5214E was an additional 1-1.2 μm in height. AZ5214E was used to make a positive mask on top of an SF-19 layer. The AZ5214E resist is an image reversal resist that can act like a positive or negative resist as discussed in Section 3.1.10.2.

Step 3: Expose AZ5214E with Electrode Pattern

In this step, the AZ5214E was used with the negative masks as a negative resist to form a positive soft mask over the SF-19 layer. AZ 5214E was exposed with the mask pattern, post exposure baked to form cross-links in the exposed areas and then flood exposed to allow removal of the area patterned with the electrode patterns.

Step 4: Develop AZ5214E

The patterned and flood exposed AZ5214E was developed using standard positive resist developer 351. As mentioned in Step 1, the electroplating bench at AFRL uses a board made specifically for electroplating 2 inch wafers. In order to connect the board to the wafer, there needs to be two electrical contact points to the seed layer—one on each opposite edge of the wafer. The wafers were placed on the board and scratched with the metal contacts to indicate the desired connection positions. The AZ5214E was cleared from the wafer's contact points for the electroplating machine using acetone on a cotton swab. As a result, the SF-19 was removed in the contact areas as well as the electrode patterned areas during the subsequent exposure and develop cycles.

Step 5: SF-19 Deep UV Exposure and Development Cycles

After the positive mask was formed, the SF-19 polyimide was patterned by repeated deep UV exposure and development steps. Three to five deep UV exposures and subsequent development steps were used to clear the polyimide. Each flood exposure exposed the SF-19 to a depth of 2-2.5 μm and each develop removed that amount of material. It was impossible to see if all of the residual material was removed so one extra exposure and develop cycle were used to be sure on MC-06 and MC-08. The wafers were all O₂ plasma ashed before electroplating to remove any remaining residual resist still left on the electrode patterned seed layer after the developments. At this point, the wafers were ready for electroplating.

Step 6: Electroplating Gold Electrodes

The electrodes were electroplated in-between SF-19 using a slow, low current density cycle. MC-07 was destroyed during this process (see Figure 4.8) because the current density was too high. The chip was badly corroded and completely useless. Three chips made it through the electroplating process intact.

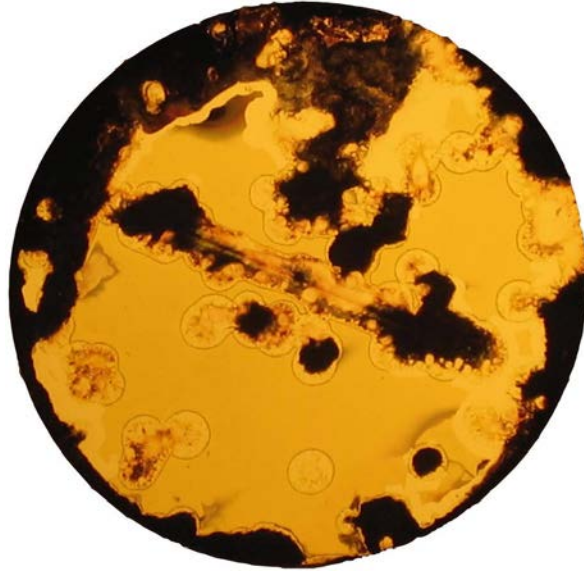


Figure 4.8 This figure shows the resulting damage to MC-07 after using an electroplating current density set too high. The electrode pattern can be seen running horizontally across this wafer. It appears that the excessive current broke through the SF-19 and AZ5214E resists in some areas.

Step 7: Photoresist Removal

After electroplating, the remaining AZ5214E was removed with acetone and the SF-19 was removed using 1165 Stripper. This left the raised electroplated electrodes on top of a seed layer. The Au from the seed layer was removed using potassium iodide. Then the Ti was removed in a bath of buffered oxide etch (BOE). After removing the seed layer, the raised electrodes and the contact points for the electroplating were the only features left on the chip. Each one of the devices ended up with a different electrode height. The heights of the microelectrodes (the highest metal) were measured by the profilometer at AFIT.

Measurements were taken from representative points on the electrodes to determine if the electrode height varied depending on the location on the wafer. From these measurements, it was clear that the electroplating process did not create electrodes with uniform heights. The heights tended to be higher near the microelectrode tip and lower near the contact pad. These measured heights were used to determine the desired SU-8 height for the next processing step. Table 4.3 shows the complete list of electrode height measurements and lists the locations of the measurements from the electroplated wafers MC-05, MC-06 and MC-08 it also displays the SU-8 height goals and the measured SU-8 heights.

Table 4.3 Electrode and SU-8 Heights on Electroplated Devices

Metal Height	MC-05	MC-06	MC-08
1. Electrode arm	4.7 μm	5.9 μm	2.3 μm
2. Neck	6.2 μm	6.8 μm	3.9 μm
3. Tip	6.5 μm	7.3 μm	4.07 μm
SU-8 Height			
Goal	6.6 μm	7.5 μm	4.2 μm
Measured	7.05 μm	7.7 μm	4.6 μm

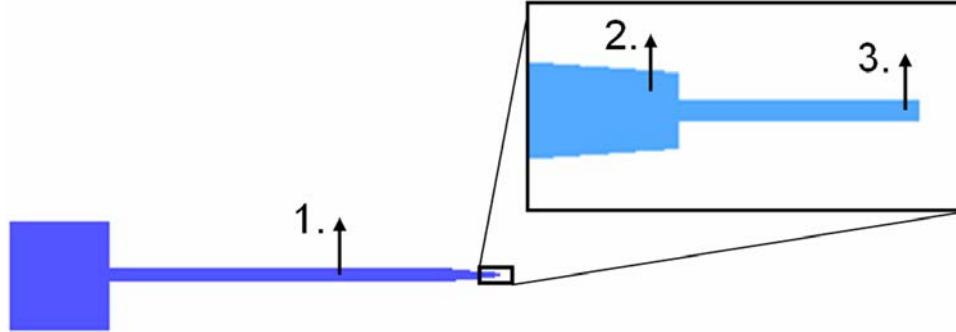


Figure 4.9 This figure shows the locations and directions of the height measurements made on the electroplated electrodes of MC-05, MC-06 and MC-08. The measurements were taken using the profilometer in the AFIT cleanroom. The positions are as follows: 1. Electrode arm, 2. Neck and 3. Tip.

Application of SU-8 at the desired height is discussed in *Step 8*. Figure 4.9 describes the locations of the electrode measurements.

Step 8: Coat Wafer with SU-8

The next step was to create the microchannel in a planar layer of SU-8. All SU-8 patterning was performed at the AFIT cleanroom using the resist spinner and the MJB3 contact mask aligner. As seen in Table 4.3, a goal height was set slightly higher than the highest measured electrode height for each device. SU-8 was spun onto each wafer slightly higher than the maximum electrode thickness for that wafer. For example, since MC-08 had a maximum metal thickness of 4.07 μm , the goal for the SU8 height on MC08 was set at 4.2 μm . For MC-06, the goal was 7.5 μm , for MC05, the goal was 6.6 μm .

Half glass slides like those shown in Figure 4.10 were used for spin speed versus height experiments to determine the exact spin speed to get the appropriate height. After spin speeds were determined, the wafers were cleaned in acetone and isopropyl alcohol then they were placed on a hotplate for a dehydration bake. Clean and dry, they were ready for

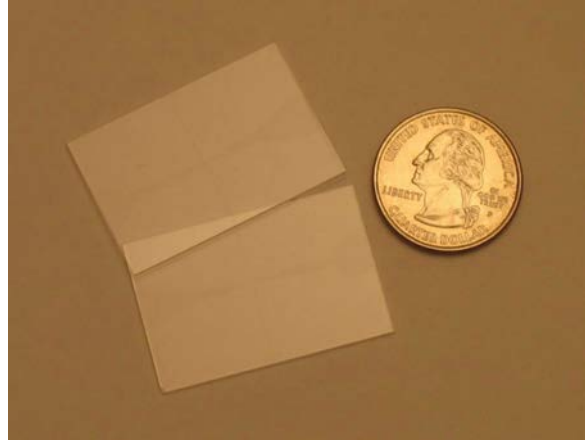


Figure 4.10 This figure shows two typical glass test samples used for the numerous resist height spin tests and cover slip bonding tests that were necessary to refine those processes. The device pattern in SU-8 can be seen faintly. A quarter is added for scale.

application of the SU-8 layer. The SU-8 patterning consists of spinning on the SU-8 at the desired thickness then soft-baking on the hotplate first at 65 °C then stepping to another hotplate at 110 °C. After the soft-bake was complete, the wafer was slowly cooled to room temp to avoid stress cracking.

Step 9: Expose SU-8 with Device Pattern

Once cooled, the wafers with the electrodes were carefully aligned using the alignment marks to the microchannel pattern on the mask and then exposed to UV light. The wafer had a tendency to move slightly during alignment causing the need to realign. One reason for the movements just as the wafer was raised into contact with the mask, microscopic raised imperfections (maybe edge bead or lumps over the electrode pattern) would bump the mask and skew the alignment by a few microns. Another cause of movements of the wafer during alignment was the mask aligner chuck. The only chuck available was designed for a 3 inch wafer. The chuck contains vacuum holes used to hold wafers in place during the contact. Using the 2 inch wafers with the 3 inch chuck tended to leave some of the vacuum holes uncovered. The uncovered holes caused air flow turbulence which jostled the wafer when the chuck's vacuum seal contacted the mask.

Many repetitions of patterning and aligning for practice chips as well as the three chips that survived the electroplating were necessary. This hard work led to a set of three

almost perfectly aligned microchannels in MC-05, MC-06 and MC-08. After the alignment and exposure, SU-8 patterning requires a post exposure bake (PEB). The UV exposure step activates an acidic reaction. The PEB adds the heat energy to the reaction that causes the molecules of the exposed portions of the SU-8 to form tight bonds with each other (cross-linking). The PEB was another step bake for 4 minutes at 65°C then 4 minutes at 110°C on another hotplate.

Step 10: Develop SU-8

When the wafers were cool again, they were developed. The SU-8 was developed for one minute in SU-8 developer and rinsed in isopropyl alcohol. This created the microchannel at the desired thickness. Next the wafers were hard baked at 150°C to harden the SU-8 and make it more resilient for use as a permanent structural layer in the microdevice. Application of the SU-8 layer was the last traditional microelectronic step. The next steps of fabricating and adhering a cover slip and fluid connection ports are somewhat unique to micro-fluidics.

Step 11: Adhere Glass Cover Slip

The next step was fabrication of the cover slip and placing it over the microchannel. There were three cover slip designs discussed in Section 3.1.12. The first design depending on a separate Pyrex cover was never attempted due to concerns about the effect of the channel length on the flow rate. The Hagen Poiseulle Law [25] given by:

$$\Delta p = \frac{8\eta l \mathbf{Q}}{\pi r^4} \quad (4.1)$$

relates volume flow rate \mathbf{Q} which has units cm^3/s with radius, r , length, l , and the applied pressure, Δp . The parameter η is the viscosity of the fluid. According to Equation (4.1), the pressure necessary to apply to the channel is proportional to the channel length assuming the volumetric flow rate and radius are fixed. Also from this law, it is clear that the relationship between pressure drop and channel radius with respect to and volumetric flow rate, \mathbf{Q} , is $\frac{1}{r^4}$. Therefore, the radius of the microchannel plays a huge role in the ability to drive fluid flow based on pressure differential. Equation (4.1) can be restated in terms of

\mathbf{U} , the average flow rate, where $\mathbf{U} = \mathbf{Q}/\pi r^2$. The restated equation [25]

$$\Delta p = \frac{8\eta l \mathbf{U}}{r^2} \quad (4.2)$$

shows that the average velocity goes as $1/r^2$. When the channel radius, r , gets small, the pressure required to keep a constant flow rate increases by a factor of $1/r^2$. Although the radius has the largest effect, length of the channel does have a linear effect on necessary pressure to drive the constant velocity flow. A smaller cover slip was necessary to keep the pressure to drive the fluid flow as low as possible.

The second cover slip design called for using a full standard number 1.5 (thickness), 22 mm X 25 mm glass cover slip. Fluid through holes were planned to be etched through the cover slip using hydrofluoric acid (HF). Small through hole patterns were included on mask 2 for this reason. Five failed attempts were made to etch through the cover slips. NR9-1000PY was used to pattern the cover slips for etching using the mask patterns. The cover slips were submerged in HF for approximately 3 minutes. Each attempt ended in completely dissolved cover slips. The problem with etching was with the photoresist patterning. An HF etch of this duration would likely need a hard-mask to block the HF from areas not being etched. Forming a hard mask was not possible due to time constraints.

The alternative to etching the through holes was to drill holes using a Dremel XPR 400 rotary tool drill press with a diamond bit. Glass clamps were made out of cleaved glass slides. The clamps were tightly held in place over a stack of about 10 cover slips at a time using Scotch tape. The lowest RPM setting (~ 2000 RPM) was used to slowly drill the holes through the glass cover slips. Vegetable oil was used to lubricate the diamond bit as it drilled. The glass clamps shown in Figure 4.11, lubrication of the bit and stacking several cover slips are all things that increased the quality of the through holes.

The drilling method had two advantages over the chemical etching process and one disadvantage. The first advantage was that the fabrication time was reduced over the chemical process. The second advantage was that design changes could be made and different hole placements could be tested without redesigning photomasks. The disadvantage is that the through holes produced in this way were jagged around the edges unlike the smooth edges expected from the etching process. The ability to change the design proved invaluable

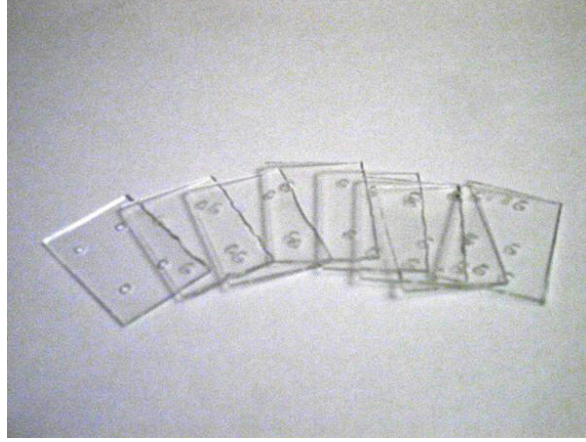


Figure 4.11 This figure shows the assortment of glass clamps used in the fabrication of cover slips. Each set of cover slips had a clamp with two pieces—one for the top and one for the bottom. Scotch tape was used to hold the clamps tight against a stack of cover slips during drilling. The clamps had hole patterns in the desired hole locations on the cover slips. The holes were used as guide holes.

because there was another late design change that effected the cover slip dimensions based on the adhesive. That design change is discussed below in Section 4.2.1.

Once the through holes were possible, the first attempt was to fabricate a full sized standard cover slip using the same hole placement and the dimensions that appear on Mask 2. When the cover slip was ready, Loctite, UV curable adhesive was used in an attempt to bond it to a test sample. A standard cover slip (with drilled through holes) was placed over the microchannel. The through holes were carefully aligned with the channel. Next, drops of Loctite were applied to the edges of the cover slips. When the adhesive met the channel border, the adhesive was cured in place by exposing it on the MJB3 contact mask aligner. Ten 99-sec exposures were performed consecutively to deliver enough energy to the adhesive to make a strong bond. A UV spot curing lamp would have been very useful at this step. Some of the problems with the adhesive overflowing into the channel can be attributed to the uncured adhesive.

Many hours in the cleanroom proved that bonding a full sized cover slip is impossible. The adhesive could not be controlled and every attempt to bond the full cover slip ended with the adhesive running into the microchannel. The main issue with the large cover slip seemed to be timing the flow of the adhesive. The adhesive flow tended to split into

two separate flows: one from the top of the electrode and one from the bottom. With a larger area to cover using the standard size cover slip, it was unpredictable which flow would get to the channel first and how much faster it would get there. Surface tension at the microchannel walls would hold the flow from entering the channel for a limited time but before the other flow would make it to the channel edge, the surface tension would be overcome by pressure and the flow would enter the channel.

Although not successful, these early trials provided hope because in some wider sections of the channel, the adhesive tended to follow the outline of the channel wall without going in. An example of the adhesive overflows is shown in Figure 4.12. The other insight gained from the first attempts was the fact that the flow rate of the adhesive could be lowered by lowering the size of the droplet applied to the cover slip. Two different droplet application methods were tested during the first cover slip attempts: the 2 mm diameter wooden end of a cotton swab, and the approximately 300 μm tips of the finest tipped tweezers available in the cleanroom. It was obvious from these trials that the smaller droplets produced using the tweezers were easier to control than the relatively enormous droplets produced with the swab. A search was conducted for smaller applicators for the next attempt. The applicator used on the final design was a 3 μm diameter probe tip from a micromanipulator system.

It was postulated that the adhesive flow could be better controlled if the distance it had to travel was reduced. The next adhesion attempt used long thin cover slips made by cleaving full size cover slips lengthwise. The original dimensions for placement of the through holes remained. Figure 4.13 shows one of the half-slide test samples with this type of cover slip design. Again due to the size of the cover slips, control of the adhesive was impossible. The long skinny cover slips did indeed make it easier to control the adhesive on the short run, however the Loctite was still unwieldy and impossible to corral along the long direction. Further reduction in size along the other direction was necessary. The third attempt consisted of even smaller cover slips. These were fabricated by cleaving full size cover slips across the short side twice. This provided a shorter path length for the adhesive to travel. The cover slips made by cleaving the short way twice allowed for much easier control of the adhesive than the original cover slips. The final cover slip designs consist of a cleaved rectangular cover slip that is approximately 18 mm X 8 mm. The distance



Figure 4.12 This micrograph shows the Loctite 3301 UV curable adhesive flowing through the micro channel. Drops of Loctite were applied to the cover slip edge to the middle right outside of the viewable picture. The adhesive is flowing from right to left. A pool of adhesive is shown collecting on the left side of the microchannel. The adhesive flowed through the microchannel (destroying it) from the right to the left.



Figure 4.13 This figure shows a test sample half slide patterned with the microchannel device pattern in SU-8 and with a cover slip that is the full 30 millimeters in length. It has through holes drilled through at the original design dimensions of 22 millimeters apart. Large droplets of adhesive were used. The channel was destroyed when adhesive flowed into the channel.

between the fluid through holes was reduced to about 7.2 mm in the final iteration. This distance corresponds to the point where the large part of the channel necks down on either side of the microchannel.

After a successful attempt at adhering a cover slip was made using a test sample, tests were then made on adhering cover slips to the test chips MC-01, MC-02, MC-03 and MC-04. Three successful practice devices MC-01, MC-02 and MC-04 were constructed during this phase. The cover slips and bonding method described above seemed to work well with these devices. MC-01 and MC-02 are both test wafers which were fabricated with the electrodes patterned into seed layers. MC-04 has no electrodes but is patterned with the device pattern in a layer of SU-8.

There were three devices constructed with the proper electrode heights and aligned channels as discussed earlier. The three devices were MC-05, MC-06 and MC-08. Due to the long lead time required to fabricate replacements for these wafers, they became very valuable to the project as time passed. Each step that these devices were subjected to were meticulously planned and tested on samples. Approximately fifty half glass slide test samples along with all four of the test devices on Pyrex (MC-01 through MC-04) were processed before cover slip bonding was attempted on the production wafers (MC-05, MC-06 and MC-08).

The first attempt of bonding using the production devices was on device MC-08. As shown in Table 4.3, MC-08 had an electrode height of 4.07 μm and a final SU-8 height of 4.5 μm . Of the three electroplated devices, this one was the least valuable to the project due to the low SU-8 height. Three quarters of the microchannel bonded correctly. During the attempt to fill the last quarter with adhesive, the Loctite ran into the micro channel by seeping along the edge of the wider channel. On MC-08 a cover slip with dimensions 22 mm X 8 mm was used.

The next attempt was with MC-06. MC-06 has an electrode height of 7.3 μm . This was probably the most important device to build because its large size may have allowed the larger cell types such as Macrophage cells to be measured. However, no flow testing results were available so this device was valued lower than MC-05 which had the most desirable channel height according to the design. The cover slip used with MC-06 was approximately



Figure 4.14 This figure shows device MC-06 during cover slip bonding. A large air bubble is shown in the upper right adjacent to the microchannel. The bottom of the picture shows the boarder between adhesive and unbonded SU-8 and glass. The adhesion process failed while attempting to fill the lower regions shown in this picture with epoxy.

22 mm X 11 mm. The first few hours of the bonding process went well and the results looked promising. However, just as in the MC-08 case, after three quarters of the cover slip was bonded, the process became more complicated. An air bubble formed that would not dissipate. Due to the importance of this chip, a very slow methodical approach was taken to address this problem. A method to disperse the bubble by applying pressure to the cover slip during the exposure was used to eliminate the bubble. After the bubble was removed, work continued to fill the remaining air gaps between the lower part of the cover slip and the SU-8 surface. At this point, adhesive again began to flow along the larger part of the channel to invade the microchannel. Figure 4.14 shows MC-06 during the adhesion process.

The large bubble visible on the left side of the micrograph was removed. The bonding process for MC-06 and MC-08 took many hours of painstaking work. Tiny droplets of adhesive were used in these processes. The applicator used was a fine ($3 \mu\text{m}$) micromanipulator probe. Adhesive was slowly applied to the edges of the cover slip in different places to precisely guide the adhesive flow. Once the adhesive invaded the microchannels on these devices, they were completely destroyed. The cover slips proved impossible to remove from the device once the adhesive had cured.

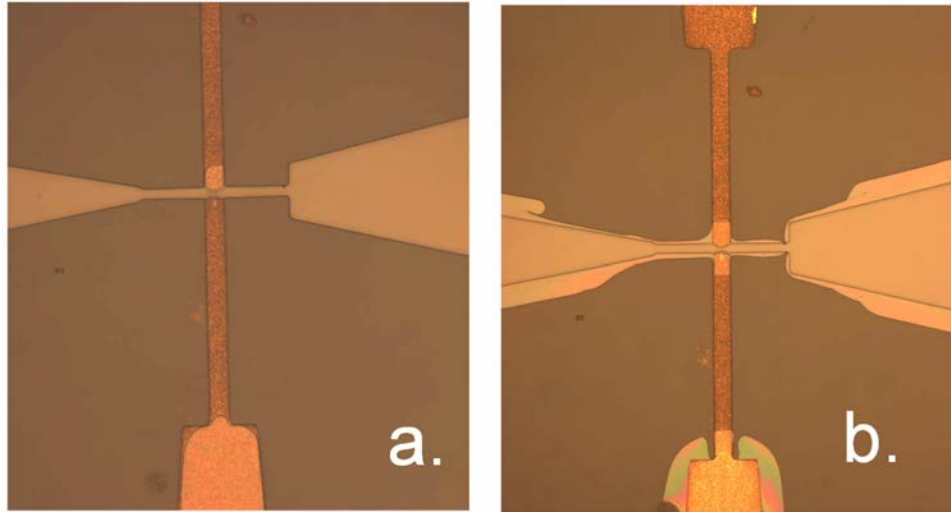


Figure 4.15 This figure shows how the adhesive leached away from the channel edge over time. The device in these micrographs is MC-05. Micrograph a. was taken directly after the UV curing phase (Ten 90 second exposures on the mask aligner) and micrograph b. was taken four days after exposure. Micrograph b. shows the adhesive border about 5 microns away from the SU-8 channel edge.

MC-05 was successfully capped with a cover slip and bonded. Insight gained from attempts to control adhesive flow on many test samples and the four test devices shown in Figure 4.16 along with MC-06 and MC-08 was used to make a good bond. Two steps led to success with cover slip bonding on MC-05: 1) the size of the cover slip was reduced to $8 \mu\text{m} \times 18 \mu\text{m}$, and 2) all four quarters of the cover slip were bonded simultaneously. The reduction in size led to better control of the adhesive. Flowing adhesive on all four quarters of the cover slip and using only one exposure phase allowed the cover slip to be removed if the adhesive flowed into the channel before it was exposed.

Figure 4.15 shows device MC-05 directly after cover slip bonding and then three days later. The adhesive migrated away from the channel walls over time. This may be due to insufficient energy applied during the curing step.

Step 12: Adhere Fluid Ports to Cover Slip

Once the cover slip was in place, fluid ports were fabricated by cutting glass tubing with a glass tube wheel cutter. The glass fluid ports were adhered to the cover slip providing access to the cover slip through holes. The same UV curable adhesive was used for bonding

the fluid ports. Large drops of adhesive were used to ensure a mechanically sound bond. The fluid ports were cured in place with ten 99 second exposures on the mask aligner.

Some flow testing was completed on the test devices before adding fluid ports. Getting a seal for the manual aspiration was difficult without the fluid ports. The fluid ports also reduced the apparent effects of evaporation that occurred during flow testing without them.

4.2.2 Devices Constructed. Ten Pyrex wafers were processed throughout the project in addition to the numerous half glass slides used to refine the processing steps. This section gives an accounting of the final outcome for each of the wafers. The first wafers to be processed were Proto_1 and Proto_2. They were patterned at AFIT using an SU-8 liftoff procedure and the electron beam evaporator. Neither Proto_1 or Proto_2 were used for testing. The next set of wafers processed was MC-01 through MC-04. This set of wafers all have electrodes processed on the seed layer using NR9 resist. The seed layer electrodes are a total of 1000 Å high including the titanium and the gold heights. These devices were useful in dry running processing steps in a more realistic way than could be achieved with the half glass slides. They were also the first set of devices to undergo flow testing. MC-01 was specially fabricated to have the same SU-8 height as MC-05. MC-01 was also better sealed around the electrodes than the other test devices which allowed fluid to flow through the channel without traveling up the electrode traces. For this reason, MC-01 was the first device to log impedance data on living cells. The impedance readings from MC-01 can not be compared directly with data from the readings on the production device because of the significantly different electrode geometry.

The second set of four Pyrex wafers feature electrodes processed with SF-19 and AZ5214E. The electrodes were electroplated to various heights shown in Table 4.3. Only one of the three wafers that began processing using this method was functional at the end. There were three wafers that were rendered useless: MC-07 was lost during electroplating due to a current overload, MC-06 and MC-08 were both lost during cover slip bonding. On MC-06 and MC-08, UV curable adhesive flowed into the microchannel blocking the passage. The electroplated electrodes were destroyed in an attempt to remove the cover slip using a combination of 1165 stripper and mechanical chipping.

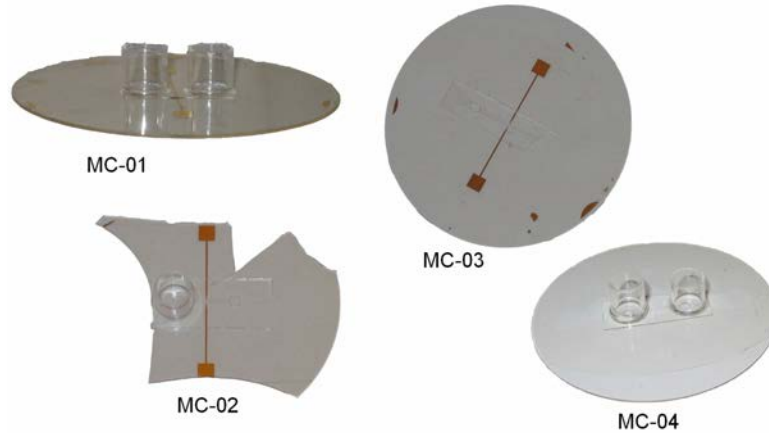


Figure 4.16 This picture shows the four test devices fabricated for this project (MC-01, MC-02, MC-03, and MC-04). The electrodes on these devices are patterned on the seed layer only. They were patterned using NR9 photoresist. Since their electrodes lacked the proper height, these devices were used as test devices during fabrication and flow testing before the fully functional chip was used. MC-04 lost its electrodes during its use as a cathode during electroplating. MC-02 was fractured while attempting to cleave the wafer close to the electrode pad.

MC-05 and MC-01 were used to take impedance measurements from a variety of substances and living and dead cells. The impedance measurement process and the data collected are discussed in Section 4.3.

4.3 Microdevice Testing

Device functionality was assessed by testing the operation of fluid flow, cell flows and recording impedance measurements. Most of the testing work was done at the AFRL, Human Effectiveness Tissue Culture lab. Macrophage cells and Jurkat T cell lines were provided for the flow testing and the impedance analysis. This section covers a description of the cell lines used and the handling procedures used with the cells, the experimental process and experimental results.

Both the test devices and the production device (MC-05) were used in the testing phase. The test devices had limited functionality because their electrodes were not electroplated. Most of the test devices had cover slips adhered in such a way that allowed fluid to flow up the electrode traces. For this reason MC-01, MC-02 and MC-04 were used for preliminary flow testing. The first flow test was performed on MC-02 with deionized water

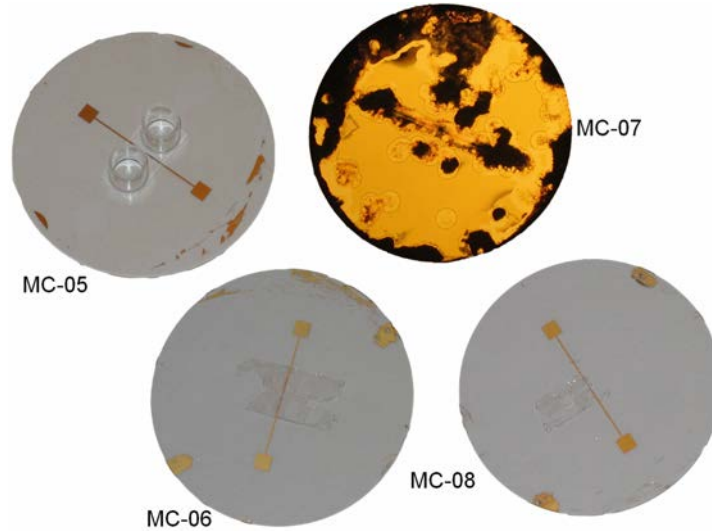


Figure 4.17 All of these devices underwent the electroplating process. The electrodes were patterned using SF-19 and AZ5214E photoresists. Three out of the four were rendered inoperable during separate fabrication steps. MC-07 was destroyed during electroplating, MC-06 and MC-08 were unfortunate losses during the cover slip adherence step. MC-05 is the only fully functional device completed. Impedance measurements were recorded on this device.

from the AFIT cleanroom. Subsequent flow testing was completed at the AFRL Human Effectiveness Tissue Culture lab with saline and cell suspension using both MC-02 and MC-04. Later, MC-01 was completed. MC-01 was less prone to fluid traveling up the electrode traces due to a better method of sealing the electrode path with the UV curable adhesive. Flow tests were continued with MC-01 using Jurkat T cells. Impedance measurements were first taken on living cells using MC-01.

4.3.1 Cell Lines . All of the cell lines used in this study were obtained from the ATCC collection. Four cell lines were discussed in this thesis: Neuro 2A, Macrophage, Jurkat T cells. Neuro 2A cells were not used beyond the collection of sizing data. Macrophages were used to collect sizing data and they were also used in the initial flow tests. Jurkat T cells were used for the first two impedance tests on cells and different Jurkat T cells were used for the final impedance tests.

Neuro 2A cells are mouse "neuronal amoeboid stem cells" [39]. The cell line was created from a tumor in an albino mouse. Neuro 2A cells are an adherent cell line. Due

to the likelihood that the cells would stick to the walls of the microchannel, they were not used for flow testing or for impedance testing.

The macrophage cells used for sizing and during the flow testing, are alveolar macrophages (mouse white blood cells which defend the lung). Macrophage are phagocytes and they are part of the immune defense. They remove foreign particles from the blood stream by engulfing them and digesting them. Macrophages tend to be large due to their role in engulfing enemies. These cells were used for initial flow testing but their size prevented them from flowing through the channel so they were not used for impedance testing. Jurkat cells are human lymphocytes derived from a 14 year old boy with leukemia in 1973 [39]. The Jurkat T cells are an immortalized cell line. The diameter of the Jurkat T cells tended to be around 8 - 10 μm so they flowed through the channel with few problems.

4.3.2 Flow Tests. Several flow tests were performed using MC-01, MC-02 and MC-04. MC-04 was used for the first formal flow testing involving live cells. MC-04 was used to determine whether the living cells would flow through the microchannels. Also important during this phase of testing was the cleaning process for the device. The microchannel tended to clog up with cell parts, proteins and other biomatter as well as glass and epoxy bits leftover from construction of the chip. A method was necessary to clean the device after use and to prepare it for reuse. Figure 4.18 shows the microchannel after the first flow tests using macrophage cells. Cell parts were left in the microchannel. Different cleaning solutions including isopropyl alcohol, mild detergent, the digestive enzyme trypsin and pressurized flow were used to clear the channel to varying degrees of success. Isopropyl alcohol damaged the epoxy so its use was discontinued. The detergent was not much more effective than plain deionized water. A trypsin solution mixed to a concentration of .25% to 1% was effective in removing cell membranes that became stuck on the glass surface. The trypsin does not damage the SU-8, the glass or the epoxy. Pressurized flow of the trypsin solution after letting the solution sit in the channel for approximately 20 minutes was most effective in cleaning the channels.

In addition to working out a cleaning process, the early flow tests assessed the ability of cells to flow through the microchannel. Work with macrophage cells showed that the channel heights on MC-04 and MC-01 are slightly too small to allow most macrophage cells

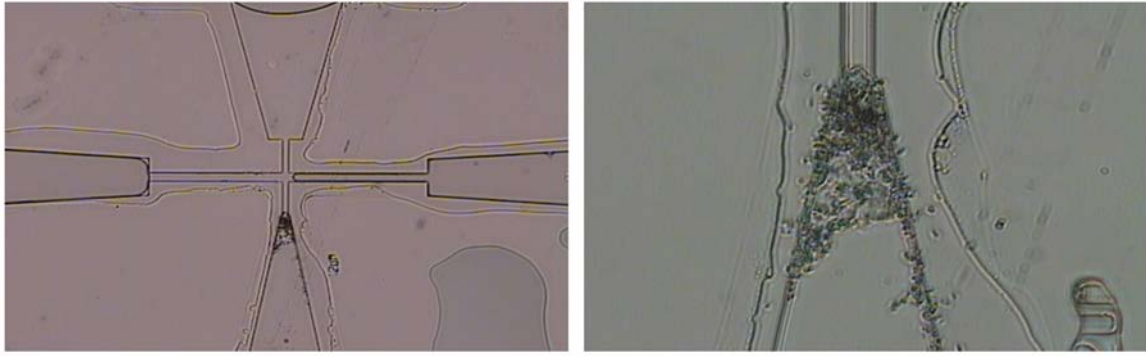


Figure 4.18 This figure shows cell organelles left in the microchannel after the first series of flow tests with MC-04. Several different approaches for cleaning the channel were tested.

to enter the channel. The macrophage flow tests were carried out using MC-04 without glass fluid ports. A rubber gasket was used to form a seal around the cover slip through holes during application of pressure to the inlet or outlet. Figure 4.19 shows that a small number of cells came very close to entering the microchannel despite the vast majority of the cells being caught at the entrance of the microchannel. Subsequent flow testing showed that Jurkat T cells (other cells available at the tissue culture lab) flowed through the channel with less problems.

4.3.3 Impedance Experiment Overview. Impedance experiments were carried out on both the MC-01 test device and the MC-05 fully functional device. Jurkat T lymphocytes were used for these impedance tests. An HP4194A impedance analyzer connected to the microdevices through a test fixture was used to make impedance measurements on various substances and living cells between the microelectrodes. The test station is shown in Figure 4.20. The impedance analyzer was controlled remotely by a laptop computer running Labview 7.0 software. A Labview program called a "virtual instrument" (VI) was written based on sample code available on the internet. The simple Labview VI program had two functions: calibrate the impedance analyzer and run an impedance sweep. The frequencies for the sweep are user selectable in the program GUI within the limits of the analyzer (1 kHz to 15 MHz). The Labview VI also sets a number of internal parameters of the impedance analyzer.

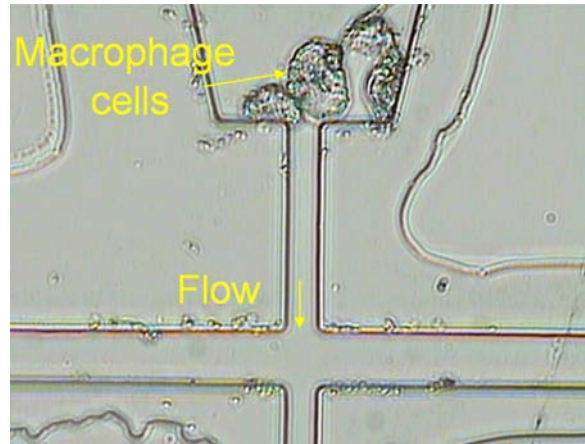


Figure 4.19 This figure displays the results of a cell flow test using macrophage cells. The direction of flow in the picture is from top to bottom. The electrode traces that run from left to right are empty on this device. MC-04 test device was used for this test. Also visible in this micrograph is the result of harsh cleaning on the epoxy. The epoxy has been eroded many microns away from the edge of the channel.

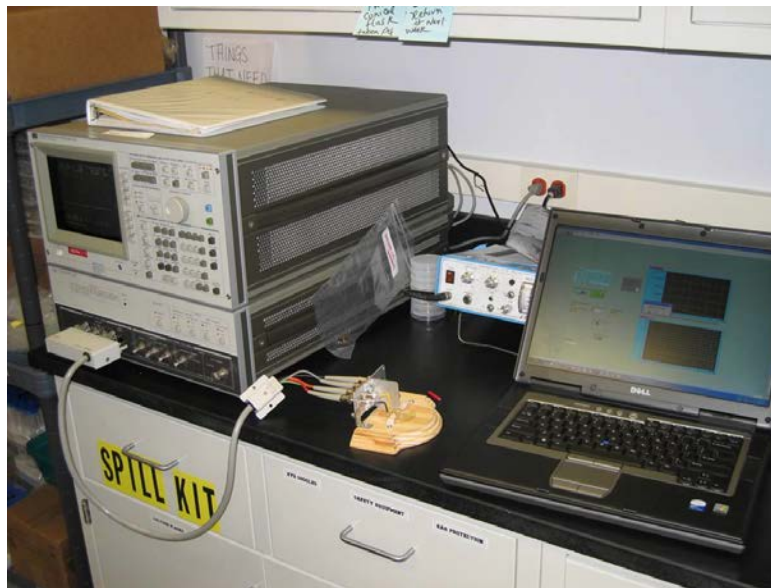


Figure 4.20 This figure shows the experimental setup used to log impedance data across a single cell. The microdevice is connected to the impedance analyzer via a test fixture and a 1 meter cable. The impedance analyzer sends the data from an impedance sweep to the laptop computer via GPIB.

4.4 Impedance Testing Results and Analysis

4.4.1 *MC-01 Procedure.* The MC-01 test device was used to collect impedance data from Jurkat cells during this experiment. As mentioned earlier, the electrodes on MC-01 are seed layer height only (about 1000 Å). Since the probes are so flat, they may not come into contact with a cell that is in the channel because the cell could be above the electrodes in the channel. Also, impedance data taken from MC-01 will not be able to be compared directly with the impedance data collected on MC-05 because the different electrode geometries will effect the stray capacitance readings. The procedure used to collect data from MC-01 is described below.

Impedance data was collected from five separate samples. The samples were measured in the following order to reduce the effects of contamination on the impedance readings: Air, Phosphate Buffered Saline (PBS), Live Cell 1, Live Cell 2 and finally Dead Cell Parts. Cells were triple washed in saline before being placed into the device. The microchannel was cleaned using a 1% trypsin solution between cell experiments and flushed three times with DIW before the next test. The dead cell parts were conglomerations of cell parts such as organelles and membranes produced when high speed cells were damaged during their trip through the microchannel. These dead cell parts were used as a separate data set due to the non-availability of other small cell lines at the time of testing.

4.4.2 *MC-01 Impedance Results.* Five sets of impedance measurements were made on the test chip MC-01. The mean of the data recorded using Air, Saline, and Live Cells are displayed in Figure 4.21. The frequency was swept from 1 kHz to 3.7 MHz during all five of these data sets. One hundred data points were collected during each sweep. Each data set was recorded 4 to six times. Interestingly, there is a separation between the data for live cells and the parts of dead cells that were measured. Also the air impedance and phase data are clearly distinguishable from the cell and saline data. Other promising findings are the close agreement of the readings from two different live cells. The close agreement here suggests that the measurements are repeatable and furthermore that they are characteristic of Jurkat T cells. The readings from the dead cell parts (listed as Dead 1) in Figure 4.21 are indeed clearly different from the live cell readings. More data must be collected to draw further conclusions.

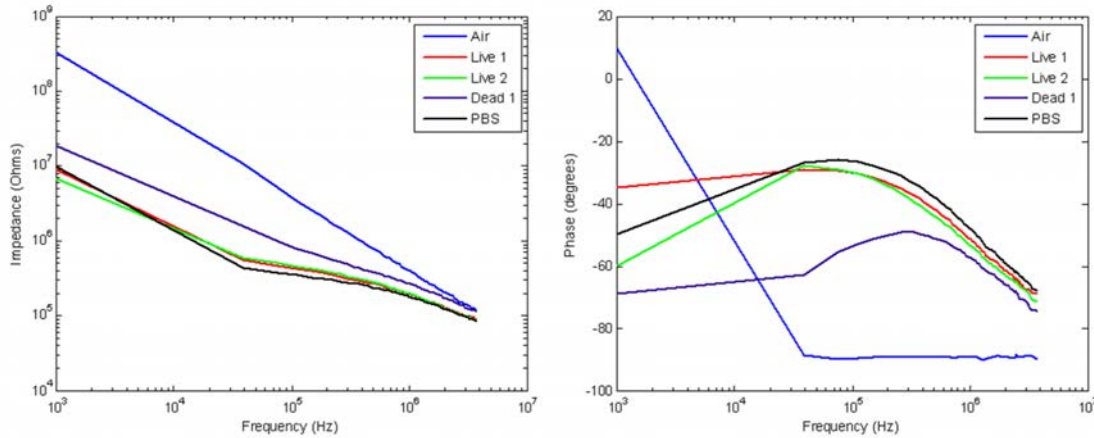


Figure 4.21 This figure shows the averages of all of the impedance readings obtained from the MC-01 test device. Five sets of readings were performed on the device: Air, two separate live Jurkat cells, cell debris (marked dead 1) and phosphate buffered saline solution.

4.4.3 *MC-05 Procedure.* Jurkat T cells were used for this experiment. The impedance data collection using MC-05 was somewhat more involved than the MC-01 test runs. There was a desire to collect more data from each sample tested in order to gain the ability to obtain some statistics. Six different samples were tested in the following order to reduce contamination effects: air, DIW, PBS, live cells then dead cells. The channel was cleaned between the cell experiments with a 1% trypsin solution and the channel was flushed with DIW three times in between all samples.

Cell suspensions were washed in saline solution three times using a centrifuge. The cell concentrations were determined by counting cells using a hemocytometer slide. The suspensions were diluted to a concentration of about 5×10^4 cells / mL. Approximately 60 μL of the diluted cell suspension was placed in the inlet port of the microdevice. Manual aspiration was applied at the inlet in order to position cells in between the measurement electrodes. Figure 4.22 shows a live cell between the measurement electrode on device MC-05. A different source of dead cells were used for this experiment. Here, a suspension of Jurkat T cells was treated with a lethal dose of CdO one day prior to the impedance readings. Trypan blue was used as a viability indicator prior to the test and found 100% of the cells treated with the CdO were dead for the test. The dead cells tended to be shrunken to around half of their normal size. The dead cell suspension was washed in saline three times just as in the live cell case. The small size of the dead cells complicated the impedance

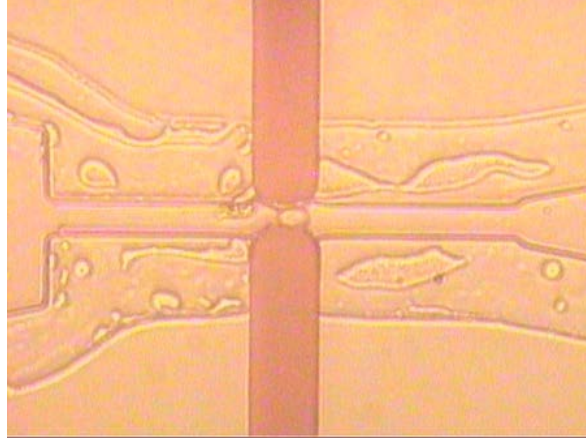


Figure 4.22 This micrograph zooms in on the microchannel of MC-05 during a cell impedance experiment. A single Jurkat T cell is shown between the microelectrodes.

readings. More than one dead cell fit between the electrodes at one time. Measurements on the dead cells were on multiple cells. This may help explain the variability observed in the impedance readings.

4.4.4 MC-05 Impedance Results. A larger frequency range was used for the impedance testing on the fully functional device MC-05. Impedance data was recorded at frequencies from 1 kHz to 15 MHz. Six data sets were recorded during this phase of experimentation. Each data set consisted of 20 - 24 impedance sweeps and each sweep contained 401 data points. Figure 4.23 shows the mean plots of the impedance and phase for each of the six data sets. The data collected during these trial runs on MC-05 contain some inconsistencies and overall appear less useful than the data collected on the test chip MC-01. For instance, Live Cell 1 and Live Cell 2 do not coincide on the magnitude and phase plots. Instead, Live Cell 2 seems to have the same impedance readings as Dead Cell 1.

There are some agreements between the two experiments however. The impedance magnitude for the dead cells are both higher than the impedance magnitudes of the live cells which is consistent with the findings from MC-01 and Figure 4.21. The readings for air magnitude and phase have a similar shape as the MC-01 data.

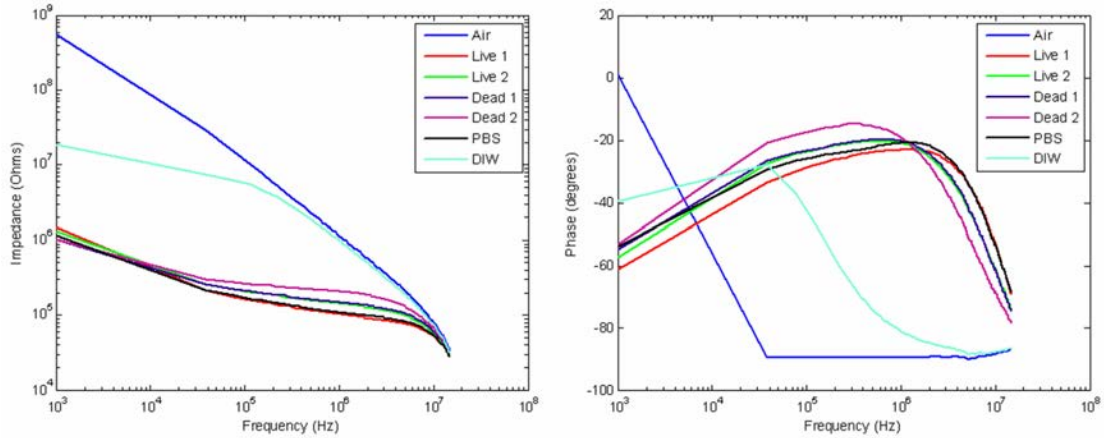


Figure 4.23 This figure shows the magnitude and phase plots from impedance data collected from six samples: air, deionized water, phosphate buffered saline, two different living cells and two different collections of dead cells. Approximately twenty impedance sweeps on each sample were averaged to produce this plot.

4.5 Results Summary

A micro-fluidic device was fabricated and the results of each of the fabrication steps were discussed. The microdevices were flow tested and procedures for making impedance measurements on the devices were developed using test devices. A test setup consisting of a computer controlled impedance analyzer, test fixture and cables was constructed. Impedance data was collected from samples of single stationary cells using the microdevice. Preliminary data suggests that there is some ability for these prototype devices to record data of sufficient information content to identify cells.

V. Conclusions and Recommendations

5.1 Project Conclusions

5.1.1 Research Goal. The goal for the research was to construct a micro-fluidic device capable of interfacing with a single cell to take impedance spectroscopy measurements which can be used for cell identification using a stochastic estimator.

5.1.2 Achievements. A microdevice successful in making contact with single cells for impedance measurements was designed, fabricated and tested. While the results are preliminary, they provide an indication that this device can be used to discriminate between cell types. Data collected from the MC-01 test device showed that live cell impedance readings were unique and repeatable.

Several design challenges such as equipment constraints, photo mask layout issues and fabrication process planning were all overcome enabling fabrication to proceed. Fabrication of the microdevice was methodical and precise yet time consuming. A fabrication process was refined using multiple prototype steps before the actual wafers were processed. Future attempts to construct similar devices at AFIT will be easier based on the experience gained with the project. Many fabrication difficulties that were encountered can be avoided with the knowledge gained. Although this project resulted in an operational microdevice, it is only the first step in the larger goal of building a multiple model adaptive estimator to handle cell identification. Work is yet to be done on that aspect of the project.

5.1.3 Design and Fabrication. Bonding for cover slips and interconnects are not necessarily common microelectronic fabrication techniques. Special knowledge and equipment is necessary to make bonds. Bonding is common to most micro-fluidic devices.

Some pieces of equipment that would have been extremely helpful and should be on hand before starting any micro-fluidic project are:

- glass tube cutters
- fluid hosing with convenient small inner diameters (possibly micro hosing)
- fluid pumps to drive fluid flow from outside
- UV curable adhesives

- UV spot curing lamps
- common photoresists and materials used for micro-fluidic fabrication like SU-8, PMGIs, PDMS
- easy access to a plasma etcher
- mask aligner chucks with diameter matching the wafers

The electroplating step created electrodes with a non uniform profile. They were higher near the channel than near the contact pads. For the next iteration of the design, this step needs to be refined so that a constant profile is maintained by lowering the current density and increasing the plating time. In addition, methods for growing the micro electrodes directly into the SU-8 mold and eliminating the SF-19 processing altogether should be investigated. This will help keep the SU-8 profile level by eliminating the bulging that occurs when SU-8 is applied conformally over the high electroplated electrodes.

5.1.4 Device Testing. A temperature and humidity controlled test fixture should be used when working with living cells. This would help ensure that the effect of the external environment on the impedance readings does not change during the experiment. The use of living cells complicated the testing setup. Proper care must be taken during the testing to keep cells viable. Cell experiments in the microchannel are time limited without the ability to provide this type of environmental control.

Fluid interconnections are extremely important in the micro device. They need to be durable, small and easy to bond. The ports that were made for this project by cutting 7 mm inner diameter glass tubing were crude but effective. Most of them withstood the mechanical stress of repeated connections and disconnections required during the testing phase. However, two devices were lost due to mechanical failure of the fluid ports. Better interconnect designs are necessary.

Early planning should be done for the ability to clean the microdevice. The extremely small microchannel tends to get clogged with various pieces of biological and non biological flotsam during experimentation. The partial solution to this problem found during this project was to apply about 50 μL of 1% trypsin solution to both ports and allow to stand for 20 minutes. This tended to loosen adhered cell based blockages. Perhaps another solution

(not an option for this project) would be to have many identical disposable microdevices such that if blockage occurs, the device can be disposed of instead of attempting to clean it.

5.2 Recommendations for Future Work

There are several areas for additional research that were identified during this research project.

5.2.1 Micro-fluidic Device Research. A thorough analysis of the electrical characterization of the test fixture and impedance microdevice should be conducted. There inevitably are stray resistances and reactances added to the analysis circuit by the test fixture and the microdevice. A better understanding of those effects would allow for more accurate data collection from a cell in the channel.

More investigations should be carried out for simpler fabrication techniques. It may be possible to rapidly fabricate different devices using a more refined process than photolithography. Impressions based microchannels may be a good option for the microchannel construction. In addition, seeking alternatives for the method of cover slip bonding should be sought.

Process yield should be much higher. The project was significantly slowed due to the low number of devices fabricated on each chip (1 device per 2 in wafer). Each step was carefully carried out such that the time to complete each fabrication step became almost unreasonable. Out of 4 wafers that entered processing, only 3 remained after the electroplating step and only 1 chip was operational (cover slip and fluid ports in place). Had higher yield been a design requirement, the research may have progressed much farther because of decreased processing time.

Knowledge of the proper equipment necessary to complete a micro-fluidic project was gained over the course of attempting to build this device. Were this project or a similar project involving micro-fluidics ever to be attempted again at AFIT, it is highly recommended that essential equipment be procured in advance. Necessary items include: glass tubing, thick photoresists used in micro-fluidics (SU-8, PDMS, SF-11 / SF-19) other

negative resists like (NR9-1000P and AZ5214E) are also invaluable to have in sufficient quantities on hand at all times.

The channel heights as fabricated ($\sim 4 - 7 \mu\text{m}$) were too low. Large macrophage cells were unable to squeeze into the channels. Cells were larger in the vertical direction than originally assumed. This prevented the testing of Macrophage cell impedance. The next design iteration should include channels that are as high as they are wide under the assumption that the cells are spherical. They should be properly sized to allow only single cells to flow through the channel while attempting to make the electrodes as flat as possible.

It was difficult to position the cells between the recording electrodes because they had freedom of movement along the channel length. The cells tended to move off of the measurement electrodes in the direction of fluid flow during the positioning process. Perhaps a better design for the purpose of impedance interrogation of a stationary cell would include a *trap* that would immobilize the cell for measurement. Mathematical impedance modeling could be done using information collected from the stationary cells. Care would need to be taken during subsequent channel design to match the stray impedance of the trap.

The fluid interconnects to the device require careful thought and are essential to the functioning of the chip. For a future project, the researchers may desire to purchase robust fluid interconnects to save time and effort.

5.2.2 Stochastic Estimator Research. Further modeling work could be carried out using devices built using the steps presented in this project. More data must be collected with these devices and work needs to be done to understand what factors affect the impedance readings taken from the devices. Separate cell lines should be tested using this device to determine the usefulness in differentiating between cell lines. The data collected during this research although preliminary, could be used to explore cell electrical models for Jurkat cells.

Since much work is necessary to produce a micro-fluidic chip for this project, perhaps a commercially available micro-fluidic device should be used at this stage. This would free up research time for working with data collected from the device.

5.3 Summary

This project was successful in implementing a device capable of reading impedance directly from cells. Further work is necessary to characterize the impedance response as a linear system and to implement an identification algorithm. The work done on this project should enable a higher fidelity model for cellular identification by interacting directly with cells. The device fabrication process that was refined during this work could jump-start future AFIT research efforts in this area.

Bibliography

1. Åberg, Peter. *Skin Cancer as Seen by Electrical Impedance*. PhD dissertation, Karolinska Institutet, 2004.
2. Ayliffe, H. Edward, et al. "Electric Impedance Spectroscopy Using Microchannels with Integrated Metal Electrodes," *Microelectromechanical Systems*, 8(1):50 to 57 (March 1999).
3. Chen, Yud-Ren and Shu-I Tu. "Impedance Spectroscopy and Biochip Sensor for Detection of *Listeria Monocytogenes*." *Proceedings of SPIE4206*. 32 – 39. SPIE, 2001.
4. Cho, Y. H., et al. "Mems-Based Biochip for the Characterization of Single Red Blood Cell." *Proceedings of the 3rd Annual International IEEE EMBS Special Topic Conference on Microtechnologies in Medicine and Biology*. 60–63. Kahuku, Oahu, Hawaii: IEEE, May 2005.
5. Clariant. *AZ5214E Image Reversal Photoresist Product Data Sheet*. Product Data Sheet, Clariant Corporation, Business Unit, Electronic Materials, 70 Meister Avenue, Somerville, NJ 08876-1252: Clariant, Circa 2000.
6. Cole, Kenneth S. "Electric Phase Angle of Cell Membrane," *Journal of General Physiology*, 641–649 (April 1932).
7. Futurrex Corp. *Negative Resist NR9-1000P*. Technical Information, 12 Cork Hill Road, Franklin, NJ 07416: Futurrex Productivity Tools. www.futurrex.com.
8. Futurrex Corp. *Resist Developer RD6*. Technical Information, 12 Cork Hill Road, Franklin, NJ 07416: Futurrex Productivity Tools. www.futurrex.com.
9. Gabrielli, Claude. *Use and Applications of Electrochemical Impedance Techniques*. Technical Report 24, Universite P et M Curie, 4 Place Jussieu, T22; 75230 Paris Cedex 05, France: Solartron Analytical, April 1997.
10. Gabrielli, Claude. *Identification of Electrochemical Processes by Frequency Response Analysis*. Technical Report 4, Universite P et M Curie, 4 Place Jussieu, T22; 75230 Paris Cedex 05, France: Solartron Analytical, March 1998.
11. Gawad, S., et al. "Micromachined impedance Spectroscopy Flow Cytometer for Cell Analysis and Particle Sizing," *The Royal Society of Chemistry*, 1:76–82 (May 2001).
12. Gerald A. Urban et al. *BioMEMS*. Microsystems, P.O. Box 17, 3300 AA Dordrecht, The Netherlands: Springer, 2006.
13. Gimsa, Jan and Derk Wachner. "A Unified Resistor-Capacitor Model for Impedance, Dielectrophoresis, Electrorotation, and Induced Transmembrane Potential," *Biophysical Journal*, 75:1107–1116 (Aug 1998).
14. Gomez, R., et al. "Microfluid Biochip for Impedance Spectroscopy of Biological Species," *Biomedical Microdevices*, 3(3):201 to 209 (2001).
15. Grimnes, Sverre and Ørjan Grøttem Martinsen. *Bioimpedance and Bioelectricity Basics*. Harcourt Place, 32 Jamestown Road, London NW1 7BY, UK: Academic Press, 2000.

16. Grimnes, Sverre and Ørjan Grøttem Martinsen. "Cole Electrical Impedance Model—A Critique and an Alternative," *IEEE Transactions on Biomedical Engineering*, 52(1):132–135 (January 2005).
17. Henkel Corporation. *LOCTITE 3301*. Technology Data sheet, www.loctite.com: Henkel Corporation, November 2004.
18. Holmes, David and Hywel Morgan. "Impedance Based Single Cell Detection Using Resonance Frequency Interrogation," *7th International Conference on Miniaturized Chemical and Biochemical Analysis Systems, 2003*: Transducer Research Foundation (Rankine Building, Oakjfield Avenue, Glasgow G12 8LT, Scotland, U. K. october).
19. <http://www.consultsr.com/resources/eis/cpe1.htm>. "What is a Constant Phase Element?." 2006. Internet Published by Research Solutions Oct.
20. Jaeger, Richard C. *Introduction to Microelectronic Fabrication, V*. Prentice Hall Incorporated, 2002.
21. Kovacs, Gregory T. A. *Micromachined Transducers Sourcebook*. 11 West 19th Street, New York, NY 10011-4285: McGraw-Hill Companies, 1998.
22. Liedtke, Rudolph J. "Principles of Bioelectrical Impedance Analysis," *Internet Article*, 1–10 (April 1997).
23. Ljung, Lennart. *System Identification Toolbox For Use with MATLAB User Guide* (Version 6 Edition). The Mathworks, March 2005.
24. Macdonald, J. Ross. "Impedance Spectroscopy," *Annals of Biomedical Engineering*, 20:289–305 (Aug 1992).
25. Madau, Marc J., "SPIE Shortcourse on Microfabrication Techniques for MicroFluidics and BioMEMS." SPIE Short Course Material, January 2003.
26. Malmivuo, Jaakko and Robert Plonsey. *Bioelectromagnetism, Online*. Oxford University Press, 1995.
27. McAdams, E. T. and J. Jossinet. "Tissue Impedance: A Historical Overview," *Physiological Measurements*, 16:A1–A13 (1995).
28. McRae, Donald A. and Mark A. Esrick. "Deconvolved Electrical Impedance Spectra Track Distinct Cell Morphology Changes," *IEEE Transactions on Biomedical Engineering*, 43(6):607–618 (June 1996).
29. Mendezaceves, Enrique. *Biological System Impedance Identification using Stochastic Estimation and Control*. MS thesis, Air Force Institute of Technology, Wright Patterson Air Force Base, Ohio, March 2006.
30. Micro Chem. *LOR and PMGI Resists*. Internet Spec Sheet, <http://www.microchem.com/products/pdf/PMGI-Resists-data-sheetV-rhccedit-102206.pdf>: Microchem Resists.
31. Micro Chem. *NANO SU-8 Negative Tone Photoresist Formulations 2-25*. Spec Sheet, 1254 Chestnut Street, Newton, MA 02464: Micro Chem, 2 2002.

32. Mohanty, Swomitra K., et al. "A Micro System Using Dielectrophoresis and Electrical Impedance Spectroscopy for Cell Manipulation and Analysis.." *The 21st International Conference on Solid State Sensors, Actuators and Microsystems.1*. 1055–1058. IEEE, June 2003.
33. Mohanty, Swomitra K., et al. "Hybrid Polymer/Thin Film Impedance System for Label Free Monitoring of Cells." *Proceedings of the 26th Annual International Conference of the IEEE EMBS*. 2561–2564. IEEE, September 2004.
34. Ogata, Katsuhiko. *Modern Control Engineering* (4th Edition). Upper Saddle River, NJ: Prentice-Hall, Inc., 2002.
35. Reid, J. Gary. *Linear Systems Fundamentals, Continuous and Discrete, Classic and Modern*, New York, St. Louis, San Francisco. McGraw-Hill Book Company, 1983.
36. Satake, Daisuke, et al. "A Sensor for Blood Cell Counter Using MEMS Technology," *Sensors and Actuators, B(83):77–81* (2002).
37. Schwan, H. P. "Linear and Nonlinear Electrode Polarization and Biological Materials," *Annals of Biomedical Engineering* (1992).
38. Senturia, Stephen D. *Microsystem Design*. 233 Spring Street, New York, NY 10013, USA: Springer Sciences and Business Media, 2001.
39. www.ATCC.org. *Neuro 2a, Macrophage and Jurkat Cell Line Descriptions*. Cell Line Product Descriptions, ATCC, March 2006.

REPORT DOCUMENTATION PAGE				<i>Form Approved OMB No. 074-0188</i>	
<p>The public reporting burden for this collection of information is estimated to average 1 hour per response, including the time for reviewing instructions, searching existing data sources, gathering and maintaining the data needed, and completing and reviewing the collection of information. Send comments regarding this burden estimate or any other aspect of the collection of information, including suggestions for reducing this burden to Department of Defense, Washington Headquarters Services, Directorate for Information Operations and Reports (0704-0188), 1215 Jefferson Davis Highway, Suite 1204, Arlington, VA 22202-4302. Respondents should be aware that notwithstanding any other provision of law, no person shall be subject to a penalty for failing to comply with a collection of information if it does not display a currently valid OMB control number.</p> <p>PLEASE DO NOT RETURN YOUR FORM TO THE ABOVE ADDRESS.</p>					
1. REPORT DATE (DD-MM-YYYY) 22-03-2007		2. REPORT TYPE Master's Thesis		3. DATES COVERED (From - To) May 2006 - March 2007	
4. TITLE AND SUBTITLE Biological Cell Identification by Integrating Micro-fluidics, Electrical Impedance Spectroscopy and Stochastic Estimation				5a. CONTRACT NUMBER	
				5b. GRANT NUMBER	
				5c. PROGRAM ELEMENT NUMBER	
6. AUTHOR(S) Schwenn, Karl, R. Capt, USAF				5d. PROJECT NUMBER	
				5e. TASK NUMBER	
				5f. WORK UNIT NUMBER	
7. PERFORMING ORGANIZATION NAMES(S) AND ADDRESS(S) Air Force Institute of Technology Graduate School of Engineering and Management (AFIT/EN) 2950 Hobson Way WPAFB OH 45433-7765 DSN: 785-3636				8. PERFORMING ORGANIZATION REPORT NUMBER AFIT/GE/ENG/07-20	
9. SPONSORING/MONITORING AGENCY NAME(S) AND ADDRESS(ES) AFRL/HEPB Applied Biotechnology Branch Attn: Dr. Saber Hussain, Email: Saber.Hussain@wpafb.af.mil Bldg 837 "R" Street Area B Wright-Patterson AFB, OH 45433-5707 DSN: 785-9517 COM: (937) 904-9517				10. SPONSOR/MONITOR'S ACRONYM(S) 11. SPONSOR/MONITOR'S REPORT NUMBER(S)	
12. DISTRIBUTION/AVAILABILITY STATEMENT APPROVED FOR PUBLIC RELEASE; DISTRIBUTION UNLIMITED.					
13. SUPPLEMENTARY NOTES					
14. ABSTRACT The integration of micro-fluidics, electrical impedance spectroscopy and stochastic estimation will lead to a device with enhanced detection capabilities. The goal of this thesis was to build a micro-fluidic electrical impedance measurement device that can be used in combination with a stochastic estimator to accurately identify living cells. A microdevice capable of making impedance measurements on individual living cells was designed and built using a series of standard microelectronic fabrication techniques. A microchannel was patterned in SU-8 photoresist between two gold microelectrodes on a two inch Pyrex 7740 wafer. The design process, the fabrication techniques for the microchannel, the fluid port fabrication and the cover slip bonding processes are described in detail. Small glass cover slips were bonded to the wafer using Loctite 3301 adhesive. Impedance measurements of single cells, in the microchannel device, were made using a HP4194A impedance analyzer. Preliminary analysis of the impedance data suggests that Jurkat cells have characteristic impedance signatures, corresponding to their cell type. The microdevice that was designed and built for this project should facilitate future work to implement a stochastic estimation algorithm capable of single cell identification.					
15. SUBJECT TERMS MICRO-FLUIDIC, SYSTEM IDENTIFICATION, ELECTRICAL IMPEDANCE SPECTROSCOPY, MICROELECTROMECHANICAL SYSTEMS, BIOELECTRICITY, BIOENGINEERING, IMPEDANCE (ELECTRICAL),					
16. SECURITY CLASSIFICATION OF:		17. LIMITATION OF ABSTRACT	18. NUMBER OF PAGES	19a. NAME OF RESPONSIBLE PERSON	
REPORT U	ABSTRACT U	c. THIS PAGE U	UU	101	Juan R. Vasquez, Lt Col, USAF (ENG)
					19b. TELEPHONE NUMBER (Include area code) (937) 255-3636, ext 7231; email: juan.vasquez@afit.edu

Standard Form 298 (Rev. 8-98)
 Prescribed by ANSI Std. Z39-18